© 2020. Published by The Company of Biologists Ltd | Journal of Cell Science (2021) 134, jcs252544. doi:10.1242/jcs.252544

RESEARCH ARTICLE

SPECIAL ISSUE: CELL BIOLOGY OF HOST–PATHOGEN INTERACTIONS

Cell-to-cell and genome-to-genome variability of adenovirus transcription tuned by the cell cycle

Maarit Suomalainen[§], Vibhu Prasad[*,§], Abhilash Kannan[‡] and Urs F. Greber[¶]

ABSTRACT

In clonal cultures, not all cells are equally susceptible to virus infection, and the mechanisms underlying this are poorly understood. Here, we developed image-based single-cell measurements to scrutinize the heterogeneity of adenovirus (AdV) infection. AdV delivers, transcribes and replicates a linear double-stranded DNA genome in the nucleus. We measured the abundance of viral transcripts using single-molecule RNA fluorescence *in situ* hybridization (FISH) and the incoming 5-ethynyl-2′-deoxycytidine (EdC)-tagged viral genomes using a copper(I)-catalyzed azide–alkyne cycloaddition (click) reaction. Surprisingly, expression of the immediate early gene E1A only moderately correlated with the number of viral genomes in the cell nucleus. Intranuclear genome-to-genome heterogeneity was found at the level of viral transcription and, in accordance, individual genomes exhibited heterogeneous replication activity. By analyzing the cell cycle state, we found that G1 cells exhibited the highest E1A gene expression and displayed increased correlation between E1A gene expression and viral genome copy numbers. The combined image-based single-molecule procedures described here are ideally suited to explore the cell-to-cell variability in viral gene expression in a range of different settings, including the innate immune response.

This article has an associated First Person interview with one of the co-first authors of the paper.

KEY WORDS: DNA virus, Nucleus, Transcription, Phenotypic heterogeneity, Cell cycle, Single virus genome, Single mRNA, Cell-to-cell variability

INTRODUCTION

Virus infections have variable outcomes, they can be lytic, chronic, persistent, latent or abortive. Lytic infections kill the host cell and release large numbers of progeny particles, whereas chronic infections continuously release infectious particles, for example hepatitis B virus infections of liver hepatocytes (Tang et al., 2018). Latent infections do not produce infectious particles, as shown with herpes viruses (Lieberman, 2016), and persistent infections give rise to low levels of progeny. Infection outcome is important because it determines the severity of the disease, yet, the underlying mechanisms are largely complex. They not only depend on cell-autonomous factors, such as the type and the innate immune status of the infected cell, but also on the environment, pro- and anti-viral agents, the immune status of the organism or the nature of the inoculum (Hendrickx et al., 2014; Oldstone, 2006). In principle, the cell-autonomous aspects of the variable infection outcomes can be addressed by studying cell-to-cell variable parameters with purified virus inocula in defined cell types. For example, cell-to-cell variable viral transcript counts and progeny yields have been observed with influenza, lymphocytic choriomeningitis, arenavirus, foot-and-mouth disease virus, herpes simplex virus 1, murine gammaherpesvirus 68 and dengue and Zika virus (Drayman et al., 2019; Heldt et al., 2015; King et al., 2018a; Oko et al., 2019; Russell et al., 2018; Xin et al., 2018; Zanini et al., 2018; Russell et al., 2019). Studies with influenza A virus revealed variability in translation and assembly of progeny particles (Bercovich-Kinori et al., 2016; Vahey and Fletcher, 2019).

Adenoviruses (AdVs) are non-enveloped, double-stranded DNA viruses that cause mild respiratory, gastrointestinal or ocular infections in immune-competent hosts and establish persistent infections, which can develop into life-threatening infections if the host becomes immuno-compromised (reviewed in Lion, 2014). Single-cell, single-particle analyses with AdV have shown further cell-to-cell heterogeneity, namely in virion binding to the cells (Stichling et al., 2018), endosomal and cytoplasmic trafficking (Suomalainen et al., 2013; Wang et al., 2017) and virion uncoating, and in the number of viral genomes (vDNA) delivered into the nucleus, the site of virus replication (Burckhardt et al., 2011; Strunze et al., 2011; Wang et al., 2013; Prasad et al., 2014; Luisoni et al., 2015; Bauer et al., 2019). The vDNA is imported into the nucleus in association with protein VII, and the protein VII-complexed vDNA is the template for early virus transcription (Chen et al., 2007; Haruki et al., 2003; Karen and Hearing, 2011; Wang et al., 2013; Xue et al., 2005; Komatsu et al., 2011; Ostapchuk et al., 2017), although partial replacement of protein VII by histones cannot be excluded (Giberson et al., 2012).

So far, AdV gene expression has been studied by classical cell-population-level assays, such as northern blots, reverse transcription quantitative PCR (RT-qPCR), microarrays or bulk cell RNA sequencing (Miller et al., 2007; Zhao et al., 2012). Following the nuclear import of AdV-C vDNA, an enhancer sequence on the left end of the viral genome activates host RNA polymerase II-mediated transcription from the E1A transcription unit promoter (Bolwig et al., 1992). Alternative splicing initially produces two different mRNAs, the 13S and 12S E1A mRNAs (Spector et al., 1978; Wilson and Darnell, 1981), which yield 289- and 243-residue multifunctional proteins that interact with numerous cellular partners and dramatically change the host cell by remodeling host gene expression, inducing S phase of the cell cycle, suppressing host innate immune responses and reprogramming cell metabolism (reviewed in Pelka et al., 2008, King et al., 2018b). In addition, the 289-residue E1A protein stimulates transcription from its own

Department of Molecular Life Sciences, University of Zurich, 8057 Zurich, Switzerland.
*Present address: Department of Infectious Diseases, Molecular Virology, University of Heidelberg, 69120 Heidelberg, Germany. ‡Present address: Institute of Microbiology, Centre Hospitalier Universitaire Vaudois, 1011 Lausanne, Switzerland.
§These authors contributed equally to this work

¶Author for correspondence (urs.greber@mls.uzh.ch)

M.S., 0000-0002-3276-3008; V.P., 0000-0001-7450-607X; A.K., 0000-0002-8502-4129; U.F.G., 0000-0003-2278-120X

Handling Editor: Derek Walsh
Received 3 August 2020; Accepted 27 August 2020

Journal of Cell Science (2021) 134, jcs252544. doi:10.1242/jcs.252544

promoter and activates transcription from the other viral early transcription units – E1B, E2, E3 and E4 – each of which yield multiple mRNAs due to alternative splicing (Binger and Flint, 1984; Glenn and Ricciardi, 1988; Hearing and Shenk, 1985; Montell et al., 1982; Zhao et al., 2014). Transcripts from the viral late transcription unit, amongst them mRNAs for the viral structural proteins, vastly increase in abundance concomitant with the onset of vDNA replication (Shaw and Ziff, 1980; Iftode and Flint, 2004; Zhao et al., 2014; Morris et al., 2010; Crisostomo et al., 2019). Single-cell and single vDNA and RNA resolution assays presented in this study further address the cell-to-cell variability of AdV infection. They reveal a highly asynchronous and heterogeneous accumulation of viral transcripts early in infection that is not due to defective viral genomes but is partly due to cell cycle effects.

RESULTS

Visualization of AdV-C5 transcripts in single cells

We used fluorescence *in situ* hybridization (FISH) with probes targeting E1A, E1B-55K and protein VI transcripts followed by branched DNA (bDNA) signal amplification to visualize the appearance and abundance of viral transcripts in AdV-C5-infected A549 lung carcinoma cells. This enables analysis of mRNAs at single-cell and single-molecule resolution (Battich et al., 2013; Yakimovich et al., 2015). Unless otherwise stated, AdV-C5 was added to cells at 37°C for 60 min at the indicated multiplicities of infection (m.o.i., virus particles per cell), and after removal of unbound virus, cells were further incubated at 37°C before fixation, staining and imaging by wide-field or confocal microscopy. The time points post infection (p.i.) included the 60-min time of virus incubation with cells. Limiting the virus incubation with cells to 60 min ensured that infection was initiated in a relatively short time window, and it enabled estimation of the actual number of virus particles entering into the cells.

Fig. 1 shows accumulation of virus transcripts in A549 cells when infection was started with an m.o.i. of 54,400 (Fig. 1B) or 13,600 (Fig. 1D–F). The m.o.i. 54,400 infection had between 6 and 173 particles per cell (median 75), and the m.o.i. 13,600 infection had between 2 and 111 particles per cell (median 26), as determined by immunofluorescence staining of cell-associated virions (Fig. 1A). In the m.o.i. 54,400 infection at 5 h p.i., cells displayed high numbers of E1A transcripts, the first mRNA transcribed from the nuclear vDNAs (Fig. 1B). The E1A probes covered the entire E1A primary transcript region and thus all E1A splice variants. The temporal control of E1A primary transcript splicing and E1A mRNA stability predominantly gives rise to 13S and 12S E1A mRNAs at 5 h p.i. (Hu and Hsu, 1997; Miller et al., 2012; Wilson and Darnell, 1981). Activation of other viral early promoters is dependent on E1A proteins (Berk, 2005), and, accordingly, the E1B-55K transcripts were generally less abundant than those of E1A at 5 h p.i. (Fig. 1B). The late protein VI transcript puncta were detected at 12 h p.i., notably with high cell-to-cell variability and abundant E1A transcripts (Fig. 1B). The E1A, E1B-55K and protein VI transcript signals in infected cells were specific, because non-infected cells had only very occasional puncta, and the puncta were suppressed by RNase A treatment, as shown for E1A. Note that individual mRNAs appeared as distinct fluorescent puncta, but the high number of viral transcripts gives rise to clusters in the maximum-projection images. A strong accumulation of E1A transcripts was observed in infected HDF-TERT cells, albeit not in all cells and with delayed kinetics, for example at 22 h p.i. (Fig. 1C). HDF-TERT are non-transformed human diploid fibroblasts immortalized by human telomerase expression (Yu et al., 2001; Zheng et al., 2016). The data indicate that the high and variable abundance of E1A transcripts is not restricted to cancer cells.

Time-resolved analysis of E1A and E1B-55K transcripts was carried out at an m.o.i. of ∼13,600 virus particles per cell. Because the high abundance of viral transcripts in individual cells precluded an automated segmentation of individual transcript puncta, mean fluorescence probe intensity per cell was used to estimate viral transcript abundance. This method is a reliable estimate for transcript abundances per cell when cells contain ≥10 transcripts (Fig. S1C). No E1A or E1B-55K transcripts were detected immediately after the removal of unbound virus, and only occasional cells displayed low numbers of E1A transcripts at the 2 h time point (Fig. 1D). E1A transcripts began to accumulate at 5 h p.i., with high cell-to-cell variability (see also Fig. S1A,B), whereas E1B-55K transcripts began to emerge in higher numbers only at around 8 h p.i. After 12 h, most cells displayed both E1A and E1B-55K transcripts. Despite considerable cell-to-cell variability, we observed good correlations in E1A and E1B-55K signals per cell at 5, 8 and 12 h p.i., with Spearman's rank correlation coefficient (r_s) of 0.63 (n=185), 0.88 (n=207) and 0.79 (n=150), respectively (Fig. 1E; approximate P values <0.000001 for all). This is in agreement with the notion that the E1B promoter is regulated by E1A protein (Berk, 1986).

The late protein VI transcripts were first detected at 12 h p.i. in a subset of cells (Fig. 1F; Fig. S1D). At the 17 h time point, about half of the cells had high numbers of protein VI transcripts, and most of them had very high numbers of E1A transcripts. By 23 h, the majority of cells contained abundant protein VI transcripts, but the cytoplasmic E1A transcripts were reduced. Whereas other time points showed relatively few E1A, E1B-55K or protein VI transcript puncta over the nuclear area (Fig. 1B,F; Fig. S1A), clustered nuclear E1A signals were apparent at 23 h. Due to further findings reported below, we assume that this nuclear E1A signal represents binding of the E1A probe to single-stranded vDNA in the replication centers. Accordingly, the nuclear area was excluded when quantifying the viral transcripts per cell in late time points (Fig. 1F). Overall, the data demonstrate that viral mRNAs accumulate in high numbers in individual infected cells, and with significant cell-to-cell variability over time.

The E1A transcript numbers early in infection correlate moderately with the number of viral genomes per cell

We next tested whether the rate of E1A transcript accumulation correlated with the number of nuclear- or cell-associated vDNAs. The rationale for this is twofold: first, not all cells bind equal amounts of virus (Fig. 1A), and, second, due to cell-to-cell differences in the overall entry efficiency, not all incoming viruses deliver their genome into the nucleus.

We used 5-ethynyl-2′-deoxycytidine (EdC)-labeled AdV-C5 (AdV-C5–EdC) and a copper(I)-catalyzed azide–alkyne cycloaddition (click) reaction with Alexa Fluor 488-conjugated azide to visualize the number of incoming vDNAs (Wang et al., 2013). Because interpretation of the results from vDNA–E1A mRNA correlation experiments is critically dependent on quantitative detection of viral genomes, we first determined the detection efficiency of the vDNA in infected cells at different time points p.i. A high percentage (∼88%) of the incoming EdC-labeled virus particles carried a detectable vDNA signal, as determined by anti-hexon antibody 9C12 and vDNA co-staining of virions in infected HeLa-ATCC mind bomb 1 (MIB1)-knockout cells (Fig. S2A). In these cells, virus entry is blocked at the nuclear pore complex because the ubiquitin ligase activity of MIB1 is needed to trigger the virus disassembly (Bauer et al., 2019).

Journal of Cell Science (2021) 134, jcs252544. doi:10.1242/jcs.252544

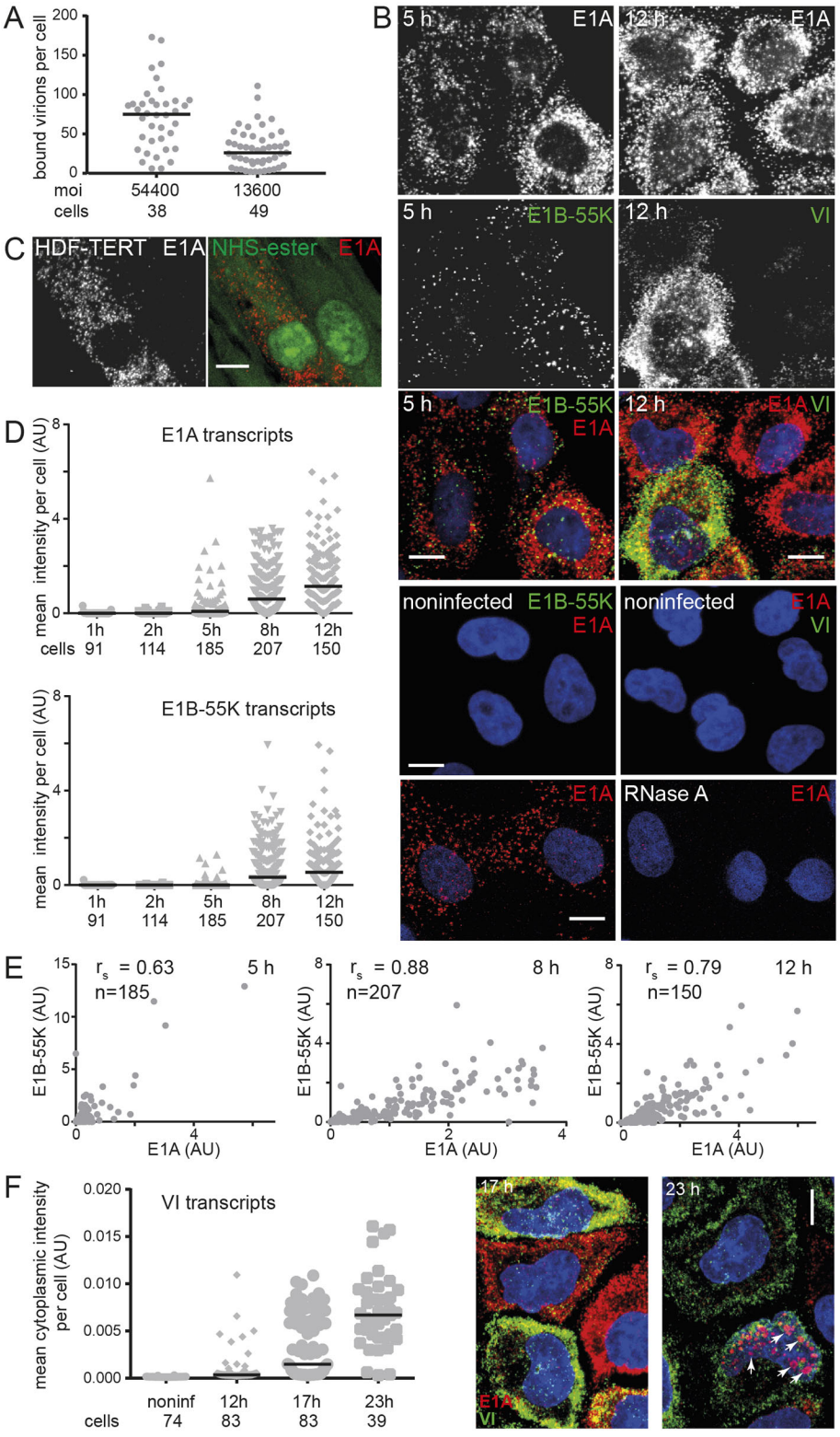

Fig. 1. Visualization of AdV-C5 E1A, E1B-55K and protein VI transcripts in infected cells using the bDNA-FISH technique. (A) Correlation between input virus amounts and number of virus particles bound to cells. Virus was added to A549 cells at 37°C for 60 min at the indicated m.o.i. (virus particles per cell). Cells were fixed after removal of unbound virus, immunostained with 9C12 anti-hexon antibody and analyzed by confocal microscopy. The scatterplot shows cell-associated viruses, one dot representing one cell. Horizontal bars represent median values and the number of cells analyzed is indicated. (B) Infected cells accumulate high numbers of viral transcripts. A549 cells were incubated with virus at m.o.i. ∼54,400 virus particles per cell, as described in A, and fixed at the indicated time points p.i. Cells were stained with probes against E1A and E1B-55K mRNAs (left-hand panel) or E1A and protein VI mRNAs (right-hand panel). RNase A treatment prior to staining removes transcript signals, as shown for E1A. (C) A high number of E1A transcripts can be detected in infected HDF-TERT cells. AdV-C5 was added to cells at 37°C for 12 h (m.o.i. ∼37,500 virus particles per cell). After removal of unbound virus, incubation was continued at 37°C for an additional 10 h before analysis. Alexa Fluor 647 NHS Ester was used for staining of cell area (pseudocolored green in the figure). (D) Timecourse analysis of E1A and E1B-55K transcript accumulation. Infected A549 cells (m.o.i. ∼13,600 virus particles per cell) were analyzed at the indicated times p.i. Mean fluorescence intensity per cell was used to quantify the abundance of E1A and E1B-55K transcripts. Horizontal bars represent median values and the number of cells analyzed is indicated. Representative images from the time points are shown in Fig S1A. (E) Correlation of E1A and E1B-55K transcripts in individual infected cells at the indicated time points p.i. The dataset is the same as in D. r_s denotes the Spearman's correlation rank coefficient (approximate *P* values <0.000001 for all three correlations). (F) Timecourse analysis of protein VI transcript accumulation. The same m.o.i. was used as in D. Horizontal bars represent median values and the number of cells analyzed is indicated. At the indicated time points p.i., cells were stained with probes against E1A and protein VI transcripts. Especially at the 23-h time point, the E1A probes not only marked the individual viral transcripts but also stained the viral replication sites in the nucleus (highlighted by arrows). All images shown are maximum projections of confocal stacks. Nuclei (DAPI stain) are blue. Scale bars: 10 µm.

We next analyzed A549 cells that had been infected with EdC-labeled AdV-C5 (m.o.i. ∼23,440 virus particles per cell), and fixed at 3 h or 7 h p.i. The number of vDNA molecules per total cell area or per nuclear area varied between cells at both time points (Fig. 2A). Median values for total cell-associated vDNA molecules (18.5 and 12 for 3 h and 7 h samples, respectively) and nuclear vDNA (16 and 8 for 3 h and 7 h samples, respectively) indicated that there was a time-dependent reduction in the number of detected vDNA molecules. This could be due to a degradation of incoming vDNAs or to a decompaction of the vDNA leading to dissipated, dim click signals. To distinguish between these possibilities, we infected A549 cells with unlabeled AdV-C5 using similar infection conditions and analyzed incoming vDNAs at 3 h and 7 h p.i. by quantitative PCR. As shown in Fig. 2B, we detected a declining

Journal of Cell Science (2021) 134, jcs252544. doi:10.1242/jcs.252544

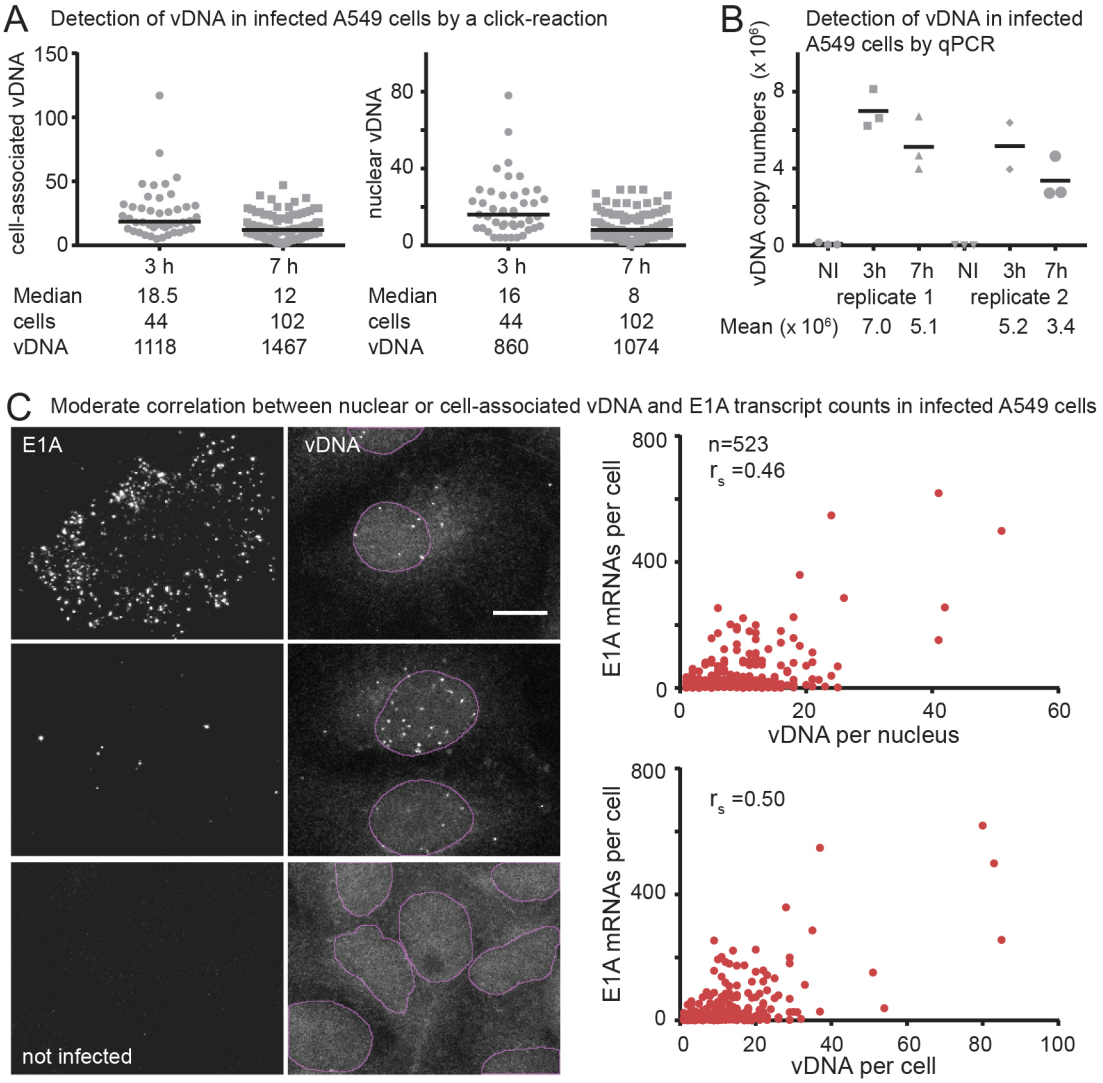

Fig. 2. E1A mRNA abundances at single-cell level early in infection only moderately correlate with vDNA counts in the total cell area or nucleus. (A) Time-dependent decrease in the number of detected vDNAs in AdV-C5–EdC-infected A549 cells. Cells were analyzed at 3 h or 7 h p.i. The incoming viral vDNA was detected by a click reaction using azide–Alexa Fluor 488. Cell area and nuclei were stained with Alexa Fluor 647 NHS Ester and DAPI, respectively. Shown are vDNA counts within the total cell area or within the nucleus area. Horizontal lines represent median values. The number of cells and vDNAs analyzed is indicated. The differences in cell-associated or nuclear vDNA numbers between 3 h and 7 h were statistically significant (cell-associated vDNA P=0.0020 and nuclear vDNA P=0.0027; Kolmogorov–Smirnov test). (B) qPCR quantification of vDNA copy numbers at 3 h and 7 h p.i. AdV-C5 infection conditions were similar to the experiment A, except the virus used was not labeled with EdC. The two biological replicates and the technical replicates for each sample are shown separately. Horizontal lines represent the mean. NI, non-infected control. (C) Comparison of E1A mRNA and vDNA counts in infected A549 cells. Cells were infected with EdC-labeled AdV-C5 (m.o.i. ∼23,440 virus particles per cell) and analyzed at 8 h p.i. Fixed cells were stained with bDNA-FISH E1A probes and the incoming vDNA was detected by a click reaction. Alexa Fluor 647 NHS Ester and DAPI stains were used for cell and nucleus area, respectively. Example images show that cells can have relatively low numbers of nuclear vDNAs and high cytoplasmic E1A mRNA counts or, vice versa, high nuclear vDNA numbers but low amounts of cytoplasmic E1A mRNAs. E1A mRNA counts at single-cell level were correlated to vDNA counts per total cell area or to nuclear area using CellProfiler. One dot represents one cell and n is the number of cells analyzed. r_s denotes the Spearman's correlation rank coefficient with approximate P values <0.000001 for both. Images shown are maximum projections of confocal stacks with nuclear outlines indicated. Scale bar: 10 µm.

trend in the vDNA numbers at 7 h p.i. compared to 3 h p.i. This implies that the time-dependent decrease in vDNA click signals in cells is in part due to degradation. Thus, the clickable vDNA can be used for estimation of vDNA numbers in cells.

To probe whether the number of vDNA molecules per cell or nucleus influences the rate of E1A mRNA accumulation, we infected A549 cells with EdC-labeled AdV-C5 (m.o.i. ∼23,440 virus particles per cell) and analyzed cells at 8 h p.i. using E1A bDNA-FISH probes and the click reaction for vDNA. As shown in Fig. 2C, the E1A transcript count per cell only moderately correlated with the number of total cell-associated or nuclear vDNA puncta. A Spearman's rank correlation test indicated r_s values of 0.50 and 0.46 for cell- and nucleus-associated vDNA, respectively (n=523, approximate P values <0.000001 for both). As few as five nuclear (nine cell-associated) viral genomes yielded a high number of E1A transcripts (>150 per cell), whereas several cells with 20–25 nuclear vDNA dots had only 5–39 E1A transcripts. Of note, because accurate segmentation was limited to ∼200 E1A puncta per cell, the values above this number are only estimates. Non-infected cells were devoid of E1A and vDNA signals. Theoretically, a high number of nuclear vDNAs could produce relatively low E1A mRNA counts if the vDNAs had to compete for scarce transcription

Journal of Cell Science (2021) 134, jcs252544. doi:10.1242/jcs.252544

factors. However, too high nuclear vDNA counts were not the reason for the observed poor correlation, because restricting the analysis to cells having between one and four nuclear vDNAs yielded a r_s value of 0.19 (n=258, approximate P value=0.0027). Low correlation between the number of E1A transcripts and the cytoplasmic area was observed (r_s value 0.23, P value <0.000001), and no significant correlation between E1A transcript numbers and nuclear area was evident (Fig. S2B). A possible population context of the cell (number of neighboring cells, relative position within a cell islet), which has been reported to be a dominant element in creating variable single-cell counts for cellular transcripts (Battich et al., 2015), could not be analyzed because AdV-infected cells are less adherent than non-infected cells and some random loss of cells was unavoidable during the RNA-FISH staining.

The effect of nuclear vDNA counts on E1A transcript accumulation was analyzed in HDF-TERT cells as well. EdC-labeled AdV-C5 was incubated with the cells at 37°C for 15 h, and after removal of unbound virus, incubation was continued for an additional 7 h before analysis. HDF-TERT cells are elongated cells with parts of the cytoplasmic region frequently extending over another cell. Therefore, cell segmentation had to be performed manually, and this explains the limited number of cells analyzed (29 cells). The result was clear though: nuclear vDNA numbers did not predict the cytoplasmic E1A mRNA counts in these cells either; for example, cells harboring ∼20 nuclear vDNAs had E1A mRNA counts ranging from 1 to 196 (Fig. S2C).

G1 cell cycle stage promotes rapid accumulation of E1A transcripts

Results shown in Fig. 2 suggest that although the number of viral genomes per cell may be one determinant for the E1A transcript accumulation early in infection, it is clear that other factors contribute as well. The cell cycle stage has been identified as an important element of heterogeneity in cellular gene expression at single-cell level (Buettner et al., 2015). We next probed whether rapid accumulation of E1A transcripts correlated with a certain cell cycle phase.

HeLa-FUCCI cells allow for easy classification of G1-phase cells (Kusabira Orange–hCdt1 expression, mKO2–hCdt1) and S-, G2- and M-phase cells (Azami-Green–hGeminin expression, mAG–hGeminin) (Sakaue-Sawano et al., 2008). Qualitative assessment of E1A transcripts in HeLa-FUCCI cells at 7.5 h p.i. suggested that the transcripts accumulated more rapidly in G1 cells than in S/G2/M cells (Fig. S3A), but no quantitative data could be obtained because spectral overlap of mKO2 and nuclear E1A transcript signals interfered with automated G1 versus S/G2/M classification of cells. We therefore used the total intensity of the nuclear DAPI signal (a proxy for DNA content) to classify cell cycle stages (Roukos et al., 2015; Ferro et al., 2017). We correlated the intensities of hCdt1 and hGeminin signals in HeLa-FUCCI cells with the DNA content distribution. As shown in Fig. 3A, low DAPI intensity marked by the G1 peak correlated with high mKO2–hCdt1 nuclear signal, and high DAPI intensity correlated with high mAG–hGeminin signal (as shown by the G2/M peak). Thus, the total intensity of nuclear DAPI signal could be used to accurately assign G1 versus S/G2/M stage to cells.

We initially correlated E1A transcript abundance and cell cycle stage using a large dataset obtained by automated wide-field fluorescence imaging of AdV-C5-infected A549 cells (m.o.i. ∼54,400 virus particles per cell) at 4 h or 7 h p.i. We used a high m.o.i. (median 75 cell-associated virus particles; Fig. 1A) in order to achieve a rapid onset of E1A expression so that the time between virus addition and analysis was short. Thus, it is not expected that a substantial number of cells would have changed their cell cycle stage during the experiment. E1A proteins induce S phase of the cell cycle and give rise to an optimal environment for viral genome replication (reviewed in King et al., 2018b).

We first compared the DNA contents of non-infected cells and the 4 h infection to ascertain that no viral manipulation of the cell cycle had yet taken place. Because the cell cycle profiles and the fraction of cells in different stages of cell cycle might be affected by unequal numbers of cells in different conditions, we randomly sampled and selected equal numbers of cells from non-infected and infected samples to draw the histograms of DNA content. These histograms, as well as the visually selected cutoffs for G1 versus S/G2/M cells, are shown in Fig. S3B. No increase in the proportion of S phase cells in the infected population was evident at this time point. The mean cytoplasmic E1A probe signal intensities were used to estimate E1A transcript abundance. When the mean cytoplasmic E1A transcript signal intensities of the cells were split into five equal frequency bins of increasing E1A intensities, both the G1 and S/G2/M cells were found in the lowest E1A bins, whereas G1 cells clearly dominated the highest E1A bins (the right-hand panel in Fig. 3B). The left-hand panel in Fig. 3B shows the distribution of E1A signals in G1 versus S/G2/M cells as a boxplot. The difference between the two classes was statistically significant according to a permutation test (P=0.0002). Furthermore, when focusing on the highest E1A expressing cells, i.e. the cells with mean cytoplasmic E1A intensities greater than 1.5× the interquartile range from the 75th percentile, 71.9% of these cells were found to be in the G1 phase, whereas only 55.8% of cells in the total cell population were G1 cells. The difference between G1 and S/G2/M cells was not an artifact of the sampling time point, because also at the 7 h time point 72.6% of the cells with highest E1A transcript numbers were G1 cells (outliers in the Fig. S3C boxplot), whereas only 57.2% of cells in the total cell population scored as G1 cells. Thus, the G1 stage favors rapid early accumulation of E1A transcripts in infected cells.

To confirm this result, we also tested E1A transcript accumulation in infected A375 melanoma cells that were either heterogeneously distributed or enriched for G1-phase cells. The cultures were first preincubated in serum-free medium for 19 h to enrich for G1 cells, AdV-C5 (m.o.i. ∼36,250) was added to the cells for 1 h, and, after removal of unbound virus, cells were further incubated either in the serum-free medium or switched to a serum-containing medium for an additional 9 h. In the serum-starved cultures, 66% of cells were in G1 phase, whereas addition of serum reduced the fraction of G1 cells to 42% as cells rapidly moved into S-phase (Fig. S3E). E1A transcript amounts per cell were determined by segmentation and counting of E1A fluorescence puncta. We excluded cells with no E1A puncta from the analysis because these might have been cells that received no virus. Both sample populations were dominated by cells with a low number of E1A puncta (Fig. S3D). A permutation test indicated that the difference between serum-starved and serum-treated samples was statistically significant (P=0.0002). The main difference between the samples was in the high E1A expressing cells. This becomes evident when focusing on cells with ≥50 E1A puncta per cell: the serum-starved, G1-enriched culture accumulated higher E1A transcript counts per cell than the serum-treated culture (Fig. 3C; P=0.0002, permutation test).

We next tested whether the more rapid accumulation of E1A transcripts in G1 cells also translated to higher E1A protein levels. We first analyzed enhanced GFP (EGFP) signals in HeLa-ATCC cells transfected with a plasmid encoding EGFP under the control of either the E1A promoter and enhancer or the cytomegalovirus (CMV) immediate early promoter and enhancer region. When the nuclear EGFP signal intensities in the E1-promoter-driven expression were split into four equal frequency bins of increasing

Journal of Cell Science (2021) 134, jcs252544. doi:10.1242/jcs.252544

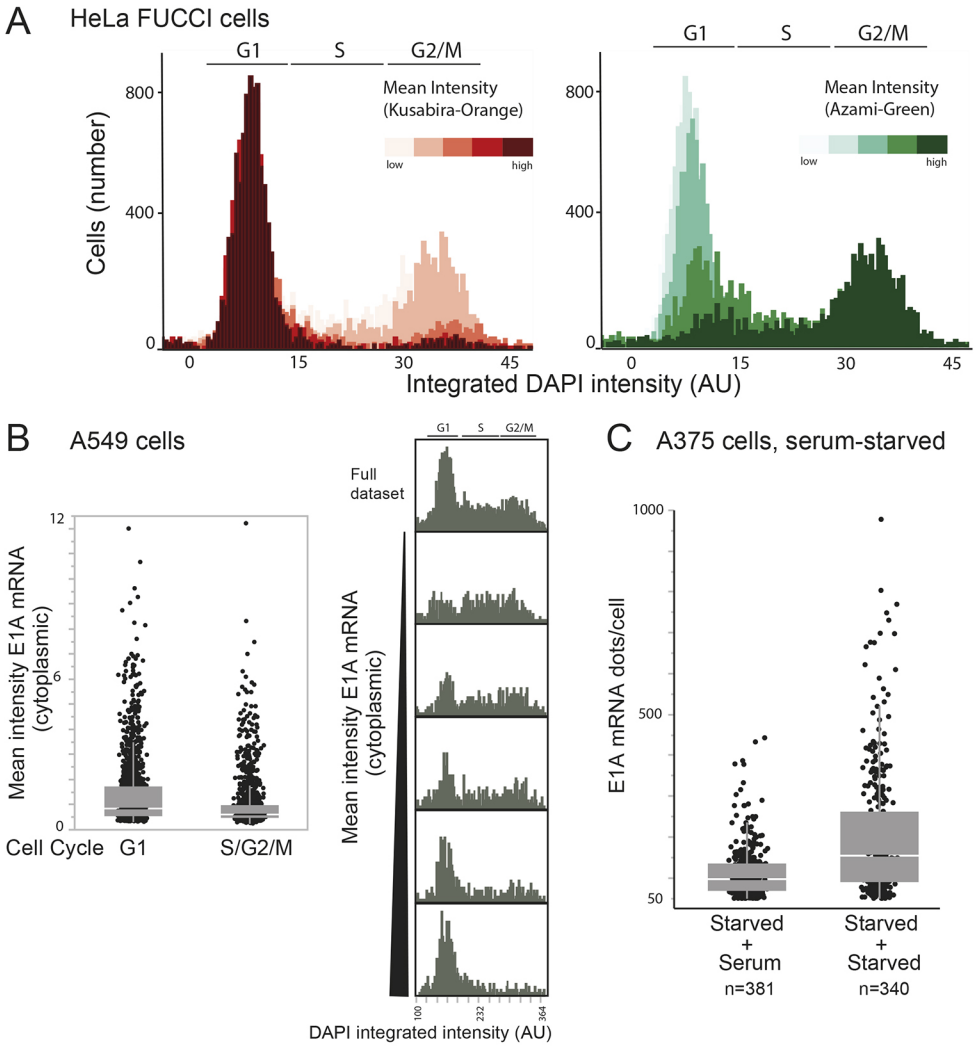

Fig. 3. G1 phase favors rapid accumulation of E1A transcripts. (A) Total nuclear DAPI signals allow accurate determination of cell cycle stages. Fixed non-infected HeLa-FUCCI cells were stained with DAPI, and the histograms show integrated nuclear DAPI intensities correlated at single-cell level to bins of increasing intensities of the G1 marker Cdt1 (Kusabira Orange, left) and the S/G2/M marker Geminin (Azami-Green, right). The increasing intensity bins of Cdt1 and Geminin mean intensity are equal frequency plots in which each bin has an equal number of cells. The integrated nuclear DAPI intensities are normalized to values 0–45. (B) E1A transcripts accumulate more rapidly in G1 cells than in S/G2/M cells. AdV-C5-infected A549 cells (m.o.i. ∼54,400 virus particles per cell) were analyzed at 4 h p.i. Fixed cells were stained with bDNA-FISH E1A probes, Alexa Fluor 647 NHS Ester and DAPI. The mean cytoplasmic E1A signal intensities were used for estimation of E1A transcript abundancies per cell. Cells were classified as G1 or S/G2/M according to total nuclear DAPI signals, and 2973 cells were randomly sampled from the total population. Of these cells, 1659 were G1 cells and 1314 were S/G2/M cells. In the left-hand panel, the mean cytoplasmic E1A signal intensities per cell in the two groups are shown as boxplots. The difference between the groups is statistically significant (permutation test; P=0.0002). In the right-hand histogram, integrated nuclear DAPI intensities of cells are correlated to mean cytoplasmic intensities of E1A transcripts. The histogram is split into five bins of increasing E1A intensities to show the correlation between E1A transcript abundancies per cell and the cell cycle phase. Each E1A intensity bin contains an equal number of cells. (C) A G1-enriched cell population shows increased numbers of E1A transcripts per cell in comparison to a cell population with a lower number of G1 cells. AdV-C5 was added to serum-starved A375 melanoma cells at 37°C for 60 min (m.o.i. ∼36,250 virus particles per cell), and after removal of unbound virus, cells were further incubated in serum-free (starved+starved sample) or serum-containing medium (starved+serum sample) for a further 9 h. Fixed cells were stained with E1A transcript probes, Alexa Fluor 647 NHS Ester and DAPI before imaging. As judged from integrated nuclear DAPI intensities, 66% of cells were in G1 phase in the starved+starved sample, and 42% were G1 cells in the starved+serum sample (Fig. S3E). Cells expressing more than 50 E1A transcripts per cell were included in the boxplot data, and the number of cells analyzed is indicated. The difference between the two samples is statistically significant (P=0.0002; permutation test). Boxplots show the interquartile range, with the horizontal gap indicating the median. Whiskers show 1.5× the interquartile range.

intensity, the ratio of G1 versus S/G2/M cells was different in the lowest and highest bins, with the highest bin having 58% of cells in G1 and 35% in S/G2/M (right-hand panel in Fig. 4A). In contrast, when EGFP expression was under the control of the CMV promoter, which is most active in S phase (Brightwell et al., 1997), 43% of cells in the highest bin were in G1 and 50% in S/G2/M (left-hand panel in Fig. 4A). The proportion difference of G1 cells in the highest bin was statistically significant (P<0.000001, two-proportion Z-test). To test E1A protein levels, we infected HeLa-FUCCI cells with AdV-C5 (m.o.i. ∼11,200) and imaged E1A-immunostained cells at 10.5 h p.i. Cells were segmented with a CellProfiler script and further sorted into early G1, G1, G1-S and S/G2/M phases using CellProfiler Analyst Classifier. As shown in Fig. 4B, E1A expression was most efficient not in G1 but in G1/S cells, which could reflect the advancement of high E1A expressing cells from G1 into S phase. However, considering the time between

Journal of Cell Science (2021) 134, jcs252544. doi:10.1242/jcs.252544

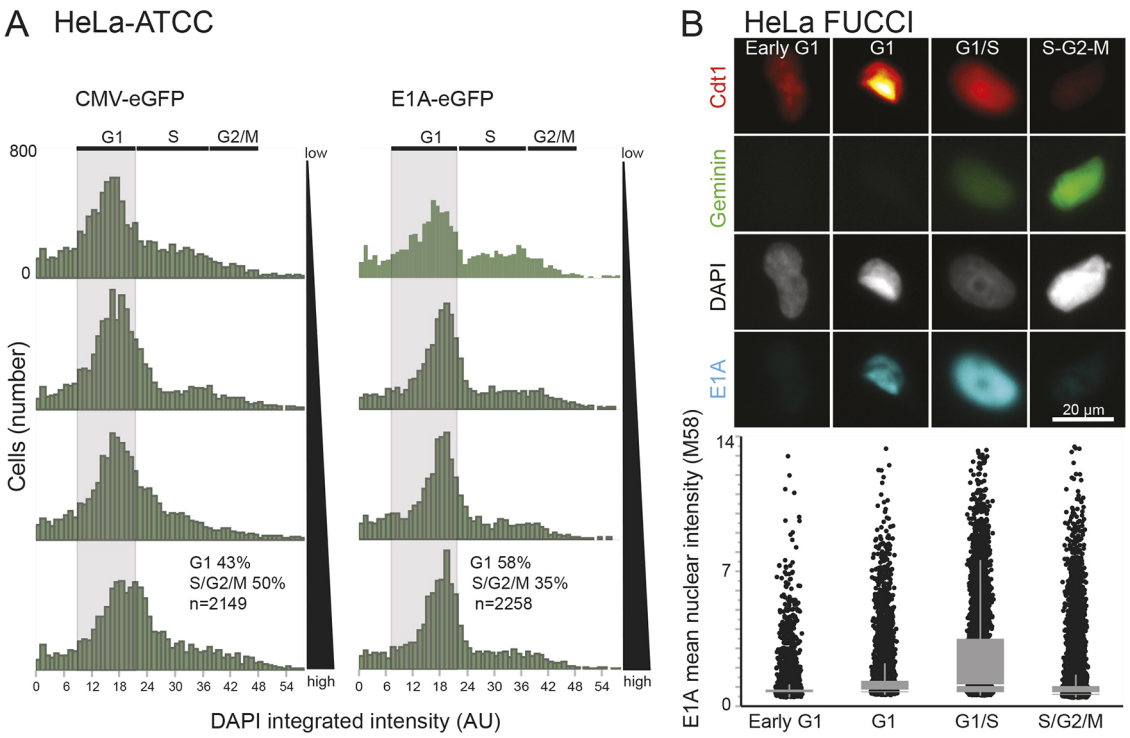

Fig. 4. G1 and G1/S phases favor high E1A protein expression. (A) High EGFP-expressing cells are predominantly G1 cells when the protein is expressed from the E1A promoter, but in CMV-promoter-driven EGFP expression, S and G2/M phases are more favorable for high EGFP expression. The data was obtained from plasmid-transfected HeLa-ATCC cells analyzed at 48 h post transfection. Histograms of integrated nuclear DAPI intensities were used to determine different cell cycle phases, and the mean nuclear EGFP intensites were mapped on the histogram. The histograms are equal frequency plots, with an equal number of cells in each EGFP bin. The proportions of G1 and S/G2/M cells, as well as the total number of cells in the highest bin, are indicated. The difference in the proportion of G1 cells in the highest bin between the CMV-promoter-driven and E1A-promoter-driven EGFP is statistically significant (P<0.00001; two-proportion Z-test). (B) Highest E1A protein expression is seen in the G1/S cells in HeLa-FUCCI infection. HeLa-FUCCI cells were infected with AdV-C5 (m.o.i. ∼11,200) and analyzed at 10.5 h p.i. using DAPI and M58 anti-E1A antibody staining. CellProfiler Analyst Classifier was used to assign cells into the indicated cell cycle phases according to their Kusabira Orange–Cdt1 and Azami-Green–Geminin nuclear signals. The mean nuclear E1A intensities in the early G1, G1, G1/S and S/G2/M cells are shown as boxplots. n=28,714. Permutation tests with pairwise comparisons indicated that differences between G1/S and other sample populations are statistically significant (P=0.0002). Boxplots show the interquartile range, with the horizontal gap indicating the median. Whiskers show 1.5× the interquartile range.

virus addition and analysis, we cannot exclude the possibility that the observed G1/S preference is at least partly due to time-dependent progression of G1 cells to G1/S.

Enhanced correlation of the E1A transcript with vDNA counts in G1 cells

Based on our finding that E1A mRNA abundance is dependent on the phase of the cell cycle, we reanalyzed the data presented in Fig. 2 by first classifying cells into G1 versus S/G2/M (Fig. S4), and then correlating cell-associated or nuclear vDNA puncta to E1A transcript numbers in the same cells. As shown in Fig. 5, E1A transcript counts per cell correlated more closely with the number of nuclear viral genomes in G1 cells than in S/G2/M cells. The r_s values were 0.52 and 0.39 for G1 and S/G2/M cells, respectively (G1 n=346 and S/G2/M n=177, approximate P values for both <0.000001). A similar trend was observed when total cell-associated vDNA was used (r_s values of 0.56 and 0.41 for G1 and S/G2/M cells, respectively, P values for both <0.000001). These results are in line with the finding that the G1 phase augments the accumulation of E1A transcripts.

High transcriptional variability of individual vDNAs in the nucleus

Despite the enhanced correlation between the nuclear vDNA and E1A mRNA levels in the G1 cells, a large fraction of cell-to-cell variability in E1A mRNAs early in infection remained unexplained. We thus assessed the amount of transcriptionally active nuclear vDNA. Cellular gene loci active in transcription have been visualized using RNA FISH targeting intron sequences (Levesque and Raj, 2013; Shah et al., 2018), or by monitoring transcriptional bursts of nascent transcripts manifested as RNA-FISH signals larger and brighter than those of individual mRNA molecules (Raj et al., 2006).

With hundreds of images analyzed, we never unambiguously detected transcriptional bursts with E1A (or E1B-55 K) bDNA-FISH probes. Whereas the introns of the AdV-C5 E1A primary transcript are too short to be visualized using bDNA FISH, the E4 primary transcript has a large intron of ∼811 nucleotides (Zhao et al., 2014). This intron is retained in the E4orf1 and E4orf2 mRNAs. We used bDNA-FISH probes against this E4 intron and EdC-labeled incoming vDNAs to identify transcriptionally active nuclear vDNAs. A549 cells were infected with EdC-labeled AdV-C5 (m.o.i. ∼23,440 virus particles per cell) and were analyzed at 16 or 18 h p.i. In contrast to E1A, E1B-55K and protein VI transcripts, relatively moderate numbers of E4 puncta were present in the cytoplasm, that is, a median number of 7 puncta per cell at 16 h p.i., and 14 puncta at 18 h p.i. (Fig. S5A).

To enhance the nuclear signals and reduce the cytoplasmic ones, we used acetic acid in the fixation buffer (Battich et al., 2013). As shown in Fig. 6A, E4 intron probes yielded nuclear puncta of

Journal of Cell Science (2021) 134, jcs252544. doi:10.1242/jcs.252544

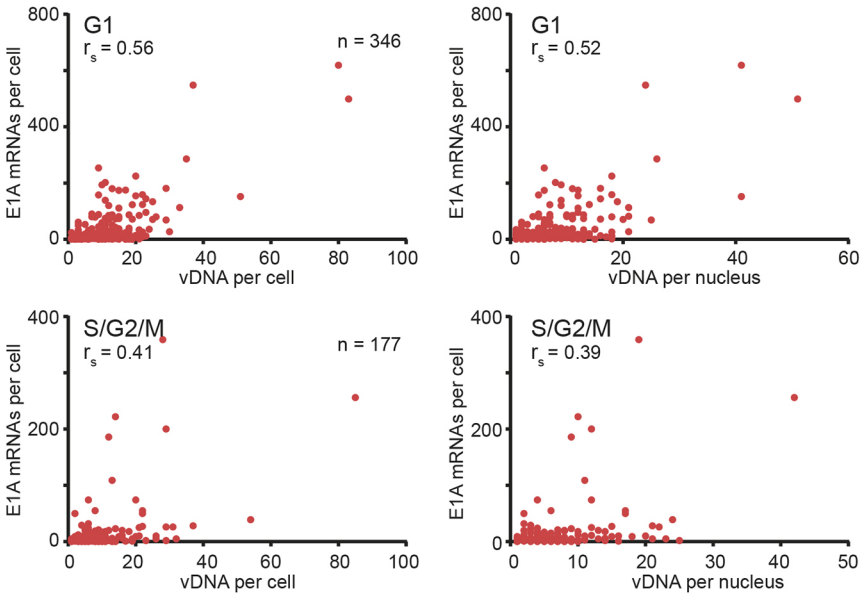

Fig. 5. Better correlation between E1A mRNA abundances per cell and total cell-associated or nuclear vDNA numbers in G1 cells than in S/G2/M cells. The dataset is the same as in Fig. 2, but cells were first classified as G1 or S/G2/M cells according to their integrated nuclear DAPI intensities (Fig. S4). The number of cell-associated or nuclear vDNA puncta were correlated to E1A mRNA numbers at the single-cell level. One dot represents one cell. r_s denotes the Spearman's correlation rank coefficient.

varying intensity at 16 h p.i., and the brighter puncta and some of the smaller puncta colocalized with vDNA click signals (indicated by red arrowheads). The nuclear E4 signals were mostly from RNA, and were suppressed by RNase A treatment (Fig. S5B,C). Plotting nuclear vDNA counts and the fraction of nuclear vDNAs positive for the E4 probe signal revealed cell-to-cell variability in the fraction of transcriptionally active nuclear vDNAs (Fig. 6A). In a minority of cells (9%) all nuclear vDNAs were associated with an E4 RNA, and 71% of these cells had nuclear vDNA counts ≤5. Cells with nuclear vDNAs totally devoid of E4 RNA constituted 32% of cells, and 82% of these cells had nuclear vDNA counts ≤5. In the rest of the cells, a variable fraction of nuclear vDNAs contained E4 RNA, and there was no obvious correlation with the number of nuclear vDNAs. Similar results were obtained at 14.5 h p.i. (Fig. S5D). Thus, vDNAs within the same nucleus display heterogeneous transcriptional activity at a given time point.

We next analyzed the progression of incoming vDNAs to the replication phase. As shown in Fig. 1F and Fig. S6A, nuclear signals with E1A transcript probes emerged only rather late in infection, and these signals were detected within the viral replication centers. When vDNA replication was suppressed by cytarabine (AraC: Fig. S6A; Schumann and Dobbelstein, 2006), which creates stalled replication foci (Triemer et al., 2018), a punctate nuclear pattern was observed with E1A probes. The nuclear E1A signals in AraC-treated cells were resistant to RNase A, but they were dampened by treatment with S1 nuclease (Fig. S6B). Thus, these foci, or the foci and ring-like structures seen in cells with active vDNA replication, originate from binding of the E1A probes to single-stranded vDNA, which is a byproduct of AdV DNA replication (Hoeben and Uil, 2013).

We used the E1A probes to monitor progression of incoming vDNAs to the replication phase. A549 cells were infected with EdC-labeled AdV-C5 (m.o.i. ∼23,400 virus particles per cell) and analyzed at 28 h p.i. AraC was added to the culture medium for the last 20 h. Representative images for colocalization of vDNA with E1A nuclear single-stranded DNA foci are shown in Fig. 6B. The majority of vDNA in the nuclear area had an associated E1A signal, but as indicated by the white arrows in the overlay images, vDNA lacking an E1A signal could be detected as well. The vDNA puncta without E1A were present in confocal slices that also contained E1A-positive vDNA puncta and thus they are unlikely to originate from cytoplasmic vDNA that appeared nuclear due to a maximum projection artifact. From 53 cells analyzed, 43 had at least one nuclear vDNA dot without an E1A signal. Thus, individual vDNAs within the same nucleus progress to the replication phase asynchronously. This was also seen in AdV-C5-EdC-infected cells not treated with AraC (Fig. 6C). Early stage AdV replication centers appear as small round puncta when visualized by an antibody directed against the vDNA binding protein (DBP), and these puncta later progress into larger globular or ring-like structures (Kato et al., 2012; Voelkerding and Klessig, 1986). The EdC-labeled viral genomes within the same nucleus were associated with either early stage or advanced replication centers (Fig. 6C).

DISCUSSION

Transcript detection in single cells

Classical infection assays report average viral gene expression levels of a cell population. Advanced single-cell technologies, including RNA FISH and single-cell RNA sequencing (scRNA-Seq) have empowered the possibility to address viral transcription heterogeneity at the single-cell level and have started to reveal significant cell-to-cell variability. scRNA-Seq permits simultaneous multiplexed virus and host transcriptome analysis. It has demonstrated large cell-to-cell heterogeneity in viral gene expression in influenza, dengue and Zika flavivirus infections and in latent HIV-1-infected human primary CD4+ T cells (Heldt et al., 2015; Steuerman et al., 2018; Zanini et al., 2018; Golumbeanu et al., 2018). scRNA-Seq, however, is technically challenging, requiring isolation of single cells, RNA amplification and complex data analysis, and it does not provide spatially resolved information in the infected cells. Single transcripts containing reporter sequences, such as a hairpin structure binding to the coat protein of bacteriophage MS2, can be tracked in live cells (reviewed in Tyagi, 2009). This, however, requires the addition of large amounts of tandem-arranged hairpins (up to 2 kb) into the

Journal of Cell Science (2021) 134, jcs252544. doi:10.1242/jcs.252544

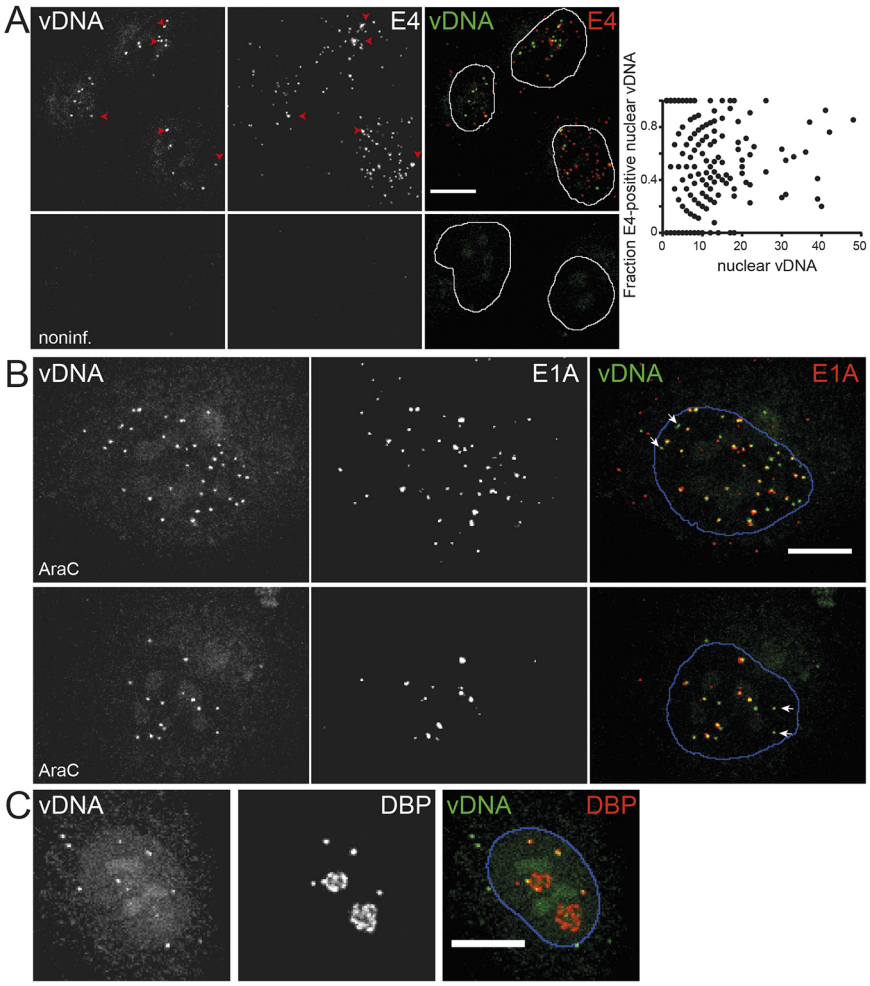

Fig. 6. vDNAs within the same nucleus display heterogeneous transcription and replication activities. (A) A549 cells were infected with EdC-labeled AdV-C5, as described in legend to Fig. 2, and analyzed at 16 h p.i. Cells were stained with intron probes targeting the E4 transcription unit, and vDNA was visualized using a click reaction. Colocalization of nuclear vDNA with E4 probe signal indicates a transcriptionally active viral genome, and the colocalization was scored from maximum projection images of confocal stacks using CellProfiler. Examples of E4-signal-positive vDNAs are indicated by red arrowheads in the images. Noninf., non-infected control. In the right-hand scatterplot, nuclear vDNA numbers are correlated to the number of E4-signal-positive vDNAs within the same nucleus, one dot representing one nucleus. Number of cells analyzed was 442. (B) Binding of E1A bDNA-FISH probes to single-stranded vDNA identifies nuclear vDNAs that have progressed to the replication stage. A549 cells were infected with EdC-labeled AdV-C5, as described in the legend to Fig. 2, and analyzed at 28 h p.i. AraC was added to the culture medium for the last 20 h. Cells were stained with E1A bDNA-FISH probes, which mark the single-stranded vDNA byproducts of stalled viral genome replication (Fig. S6), and the infecting vDNAs were visualized using a click reaction. Two representative cells are shown. The majority of nuclear vDNAs at this time point p.i. had progressed to the replication stage, as indicated by colocalization of vDNA dots with E1A probe signals, but vDNAs devoid of E1A signal were commonly detected as well (white arrows in the overlay image). (C) vDNAs within the same nucleus start replication asynchronously. A549 cells were infected with EdC-labeled AdV-C5 in the absence of AraC. Viral replication centers were visualized using an anti-DBP antibody, and incoming vDNAs using a click reaction. Small DBP-positive puncta indicate early-phase replication centers, and both these early-phase, as well as the later-phase globular or ring-like replication center structures were associated with incoming vDNAs. All images shown are maximum projections of confocal stacks. Nuclei outlines were drawn from DAPI-stained nuclei. Scale bars: 10 µm.

viral genome, which could interfere with the replicative ability of the virus.

To bypass all these shortcomings, we developed a novel combination of image-based single-molecule assays for virus infection. We exploit the subcellular information of chemically tagged fully replicative single viral genomes, bDNA-FISH assays reporting viral transcripts and single-virion fluorescence assessing the particle location. Using this approach, we demonstrate that the rate of accumulation of the first AdV-C5 mRNA, E1A, only moderately correlates with the number of viral genomes in the nucleus. Furthermore, the data show that in some cell nuclei but not others the vDNAs have non-uniform transcriptional activity and progress asynchronously into the replication phase. Our results indicate that the E1A, E1B-55K and protein VI viral transcripts accumulate in high numbers in infected cancer cells and non-transformed cells, such as HDF-TERT cells, typically reaching levels >200 transcripts per cell, in agreement with population-based assays (Flint and Sharp, 1976; Zhao et al., 2012; Crisostomo et al., 2019). In comparison, only about 5% of HeLa cell mRNAs have mean transcript numbers larger than 200 per cell (Battich et al., 2013).

Single-molecule RNA-FISH assays are convenient to use, because assay systems are commercially available (ViewRNA, RNAscope, Stellaris), RNA molecules are detected without

isolation or enzymatic amplification with single-molecule and subcellular resolution, and data analysis is straightforward, with open-source tools, such as CellProfiler and Knime, available. RNA-FISH technologies have been used to visualize, for example, the incoming or reverse transcribed HIV-1 genomes (Peng et al., 2014; Puray-Chavez et al., 2017), for monitoring lymphocytic choriomeningitis mammarenavirus RNA species during acute and persistent infections (King et al., 2018a) or for probing the genome segment ratios and packaging mechanism of the tri-segmented bunyavirus Rift Valley fever virus genome (Wichgers Schreur and Kortekaas, 2016). However, RNA-FISH assays also have drawbacks; for example, a relatively long target sequence is required for a bright signal, which makes mRNA splice-variant detection challenging. Another drawback is the limited number of targets that can be simultaneously uncovered, although different schemes for sequential rounds of hybridization have been developed to multiplex single-cell RNA FISH (Lubeck et al., 2014; Chen et al., 2015). However, such procedures are not necessarily applicable for virus infections if cells do not remain firmly attached to imaging plates, as in the case of AdV-C5 infection.

Low correlation of viral genome and transcript abundance

Our studies underscore that viral genomes within a single nucleus can give rise to variable amounts of viral mRNA transcripts. For example, similar high amounts of E1A mRNAs (>100) were observed in cells with less than ten or more than 40 nuclear vDNAs. Conversely, examples of cells with E1A transcripts less than 20 were easily found in cells with nuclear vDNA counts of ∼20, although in general, cells with high nuclear vDNA counts contained high E1A transcript numbers at 8 h p.i. At present, the molecular basis of the variability between viral genomes and E1A expression early in infection is unknown. Transcription from the E1A promoter is subject to both positive and negative regulation by cellular factors, and, in addition, E1A proteins, primarily the long 289-residue isoform, increase E1A transcription through a positive feedback loop (Berk, 1986; Zheng et al., 2016; King et al., 2018b; Prasad et al., 2020). Abundance and intracellular localization of the cellular regulators of E1A transcription could influence the rate at which individual cells accumulate E1A transcripts. This suggests that effective local concentrations of transcription regulators within the immediate vicinity of the vDNA, rather than the overall cellular or nuclear concentrations, will determine the transcriptional output from the viral promoters. Indeed, several reports have provided evidence that transient, dynamic spatiotemporal clustering of transcription regulatory factors and RNA polymerase II play an important role in transcription output from cellular promoters (Cho et al., 2016; Cho et al., 2018; Chong et al., 2018; Cisse et al., 2013; Heist et al., 2019; Li et al., 2019; Sabari et al., 2018).

Enhanced E1A transcript abundance in G1 cells

What has also become clear from our study is that the cell cycle phase accounts for some of the cell-to-cell variability in AdV transcription. Manipulation of the cell cycle is common in infections (Bagga and Bouchard, 2014). For example, the E1A proteins, together with key cellular interaction partners, push the host cell into S phase for optimal support of viral genome replication (Ben-Israel and Kleinberger, 2002; King et al., 2018b). Here, we have shown that G1 cells promoted the rapid accumulation of E1A transcripts. The underlying reasons are currently unknown, but could involve enhanced viral transcription or decreased E1A mRNA decay, the latter reported to be cell-type dependent (Lavery and Chen-Kiang, 1990).

Variable transcription and replication activities of viral genomes

Individual vDNA molecules within the same nucleus displayed varied transcriptional activity when transcription was visualized by colocalization of EdC-labeled vDNA click signal with a probe against an intron from the viral E4 transcription unit, the only early viral intron that is long and abundant enough to be detected by the RNA-FISH procedure. This gave a snapshot view of the E4 promoter activity, and it did not reveal whether the inactive vDNAs exhibited transient or prolonged transcriptional inactivity, or whether other promoters were active on the vDNA. Live-cell assays with uninfected cells have shown that transcription of cellular genes is discontinuous, with periods of bursts followed by inactive periods of variable duration (Larsson et al., 2019; Rodriguez et al., 2019). This is in agreement with local transient clustering of transcription regulatory factors and RNA polymerase II. If AdV transcription followed a similar pattern and if the transcription silent periods were short, then our snapshot assay might overestimate the intranuclear heterogeneity of vDNA transcription activities. However, viral genomes in the same nucleus not only showed transcriptional variability but also high replicative variability, as indicated by the progression of individual EdC-labeled incoming vDNAs into replicative centers containing single-stranded DNA, a byproduct of viral genome replication. This emphasizes that vDNAs within the same nucleus are subjected to a differential regulation. In agreement, considerable heterogeneity in vDNA and viral mRNA contents in post-replication phase AdV-C5-infected cells has been observed with single-cell analyses of vDNA and viral transcripts using a padlock-probe-based rolling circle amplification method (Krzywkowski et al., 2017).

Overall, it is likely that the three-dimensional host genome architecture around the vDNA affects the transcriptional output from the viral genome. This notion is in line with a recent Hi-C and vDNA capture analysis of AdV-C5-infected human hepatocytes, where the viral genome preferentially interacted with transcription start sites and enhancers of active cellular genes, including genes that are upregulated during infection (Moreau et al., 2018). Because the Hi-C measurements are population-averaged snapshots and do not give information on the dynamics of the contacts, it is unknown whether AdV usurps enhancers of cellular genes to promote its transcription in addition to using its own enhancers, or whether the viral enhancers create transcriptional hubs that benefit nearby cellular genes. Such questions can now be addressed using the image-based single-cell, single-molecule assays described here.

In summary, our study demonstrates that the progression of AdV infection is variable at the single-cell and single-genome levels, an observation that might apply to many other infections (Drayman et al., 2019; Heldt et al., 2015; King et al., 2018a; Oko et al., 2019; Russell et al., 2018; Xin et al., 2018; Zanini et al., 2018). The strategy introduced in this study is highly versatile, and can be easily adapted to other viruses, transgenes from viral vectors or non-viral transcripts, including for identification of outlier phenotypes in the innate response of cells against viruses. We envision further technical developments, such as assays for live measurements of incoming viral genomes, transcriptional output and transcription regulatory factor dynamics at single viral genomes in the nucleus (Pied and Wodrich, 2019). Improvements in single-molecule detection methods (Li et al., 2019) might make these assays feasible in the near future.

MATERIALS AND METHODS

Details of reagents and resources are provided in Table S1.

Journal of Cell Science (2021) 134, jcs252544. doi:10.1242/jcs.252544

Cells

Two different clones of human lung epithelial carcinoma A549 cells were used in the study: our laboratory's old A549 clone (experiments shown in Fig. 1; Fig. 3B; Fig. S1A,B,D; Fig. S3B,C; and Fig. S6A) and A549 from the American Type Culture Collection (ATCC; experiments shown in Figs 2, 5 and 6, Figs S1C, S2B, S4, S5 and S6B). Highly-polymorphic short tandem repeat loci profiling indicated ∼95.1% similarity for these two A549 clones. A549 cells were maintained in DMEM (Sigma-Aldrich, D6429) supplemented with 7.5% fetal calf serum (FCS; Gibco/Thermo Fisher Scientific, 10270106) and 1% non-essential amino acids (Sigma-Aldrich, M7145). HeLa cells were from ATCC (clone CCL-2) and HeLa-FUCCI cells, kindly provided by Cornel Fraefel (University of Zurich, Zurich, Switzerland), were originally obtained from Atsushi Miyawaki (Sakaue-Sawano et al., 2008). HeLa-ATCC MIB1-knockout cells have been described previously (Bauer et al., 2019). Immortalized human diploid fibroblast HDF-TERT cells expressing the catalytic subunit of telomerase were kindly provided by Patrick Hearing (Stony Brook University, Stony Brook, NY) and Kathleen Rundell (Northwestern University, Evanston, IL; Yu et al., 2001). Melanoma A375 cells, kindly provided by Alex Hajnal (University of Zurich, Zurich, Switzerland), were originally from ATCC (CRL-1619). HeLa and HeLa-FUCCI cells, as well as HDF-TERT and A375 cells were maintained in DMEM supplemented with 10% FCS and 1% non-essential amino acids.

Viruses

AdV-C5 viruses were grown in A549 cells and purified on CsCl gradients as previously described (Greber et al., 1993). EdC-labeled AdV-C5 was produced in A549 in the presence of 2.5 µM EdC added at 14 h p.i. (Wang et al., 2013). EdC was from Sigma-Aldrich (T511307). Absorbance measurements at 260 nm were used for determination of number of virus particles per ml (Sweeney and Hennessey, 2002).

RNA FISH with bDNA signal amplification

A549 cells were seeded at a density of 6000 per well in a 96-well imaging plate (Greiner Bio-One, 655090) and grown for two days. AdV-C5 was incubated with cells at the indicated multiplicities of infection (m.o.i.; two cell doubling times were included in the m.o.i. calculations) at 37°C for 60 min in DMEM supplemented with 0.2% BSA and penicillin-streptomycin. After removal of unbound virus, incubation was continued in DMEM supplemented with 7.5% FCS, 1% non-essential amino acids and penicillin-streptomycin for the indicated times (the time post infection includes the 60-min virus incubation with cells). Cells were fixed with 3% PFA in phosphate-buffered saline (PBS) for 30 min at room temperature, washed twice with PBS, dehydrated by sequential incubations in 50% ethanol for 2 min, 70% ethanol for 2 min, 100% ethanol for 2 min and plates were stored in 100% ethanol at −20°C until proceeding with RNA-FISH staining. An Affymetrix QuantiGene ViewRNA HC screening assay system (available from Thermo Fisher Scientific) was used for single-molecule RNA FISH with bDNA signal amplification (Battich et al., 2013; Yakimovich et al., 2015). Cells were rehydrated by sequential incubations in 70% ethanol for 2 min, 50% ethanol for 2 min and PBS for 10 min, permeabilized by a 5-min incubation in 0.2% Triton X-100 in PBS and washed twice in PBS. RNA FISH with bDNA signal amplification was performed according to a protocol recommended by the manufacturer using custom-made probes against AdV-C5 E1A mRNAs (type 1 probes, Alexa Fluor 546, probes were made against the sequence between the AdV-C5 genome map positions 551–1630), E1B-55K mRNA (type 4 probes, Alexa Fluor 488, probes were made against the sequence spanning the AdV-C5 map positions 2421–3495), protein VI mRNA (type 4 probes, Alexa Fluor 488, probes were made against the sequence spanning the AdV-C5 map positions 18040–18700) and E4orf1/orf2 mRNAs/introns (type 1 probes, Alexa Fluor 546, probes were made against the E4 transcript region spanning the AdV-C5 map positions 35547–34735). Nuclei were stained with DAPI (4′,6-diamidino-2-phenylindole; 1 µg/ml in PBS) for 20 min at room temperature, and Alexa Fluor 647 NHS ester (A20006, Thermo Fisher Scientific; 0.5 µg/ml in PBS for 10 min) was used for staining of the cell area. To confirm that the cytoplasmic probe signals represented viral transcripts, samples were treated or not with 65 µl of 50 µg/ml RNase A in PBS per well for 30 min at room temperature after permeabilization with Triton X-100, washed three times with PBS and, prior to proceeding to the RNA-FISH staining, cells were again fixed with 3% paraformaldehyde in PBS for 15 min at room temperature. Imaging was carried out with a Leica SP5 confocal laser scanning microscope (Fig. 1 experiments) using 63× magnification oil objective (numerical aperture 1.4) and zoom factor 2. Stacks were recorded at 0.5-µm intervals with sequential acquisition using between-frames switching mode and typically 4× frame averaging for the RNA-FISH signals. Representative images shown are maximum projections of confocal stacks, and images were processed with Fiji (Schindelin et al., 2012), applying the same changes in brightness and contrast to all image groups in the series. CellProfiler (http://cellprofiler.org; Carpenter et al., 2006) pipelines were used to score mean cell-associated transcript intensities at single-cell level from maximum projections of image stacks. The resulting data were sorted using the KNIME Analytics Platform (https://www.knime.com/knime-analytics-platform), and background, non-infected cell mean cell-associated fluorescence signals were subtracted from infected cell values. Alternatively, when the majority of cells contained fewer than ∼200 transcripts per cell, the transcript abundancies per cell were determined by segmentation and counting of fluorescence puncta per cell using CellProfiler pipelines. GraphPad Prism (GraphPad Software, La Jolla, CA, USA) was used to create the scatterplots.

For analyzing E1A transcripts in infected HDF-TERT, cells were seeded at a density of 8000 per well in a 96-well imaging plate and grown for two days. AdV-C5 was incubated with the cells at 37°C for 12 h (m.o.i. ∼37,500 virus particles per cell) in DMEM supplemented with 10% FCS, 1% non-essential amino acids and penicillin-streptomycin. After removal of the inoculum medium, incubation was continued at 37°C for an additional 10 h before cells were fixed and stained for E1A mRNAs and cell area as described above. Imaging was carried out with a Leica SP5 confocal laser scanning microscope as described above.

Estimating number of virus particles entering into cells

A549 cells grown on a 96-well imaging plate (Greiner Bio-One, 655090) were incubated with AdV-C5 (m.o.i. ∼54,400 or 13,600 virus particles per cell) at 37°C for 60 min in DMEM supplemented with 0.2% bovine serum albumin (BSA, Sigma-Aldrich, A9418) and penicillin-streptomycin (Sigma-Aldrich, P0781, final concentration penicillin 100 units per ml and streptomycin 0.1 mg per ml). After removal of unbound virus, incubation was continued in DMEM supplemented with 7.5% FCS, 1% non-essential amino acids and penicillin-streptomycin for 5 min at 37°C. Cells were placed on ice and stained with Alexa Fluor 647-conjugated wheat germ agglutinin (Thermo Fisher Scientific, W32466; 4 µg/ml in cold RPMI-1640 medium, Sigma R7388) for 1 h in the dark for cell outlines. Cells were subsequently fixed with 3% paraformaldehyde in PBS for 20 min at room temperature and stained with mouse 9C12 anti-hexon antibody (Varghese et al., 2004; 9C12 antibody, developed by Laurence Fayadat and Wiebe Olijve, was obtained from Developmental Studies Hybridoma Bank developed under the auspices of the National Institute of Child Health and Human Development; 1:40 dilution of clarified hybridoma culture supernatant), secondary Alexa Fluor 488-conjugated goat anti-mouse (Thermo Fisher Scientific, A11029; 4 µg/ml) antibodies and 1 µg/ml DAPI, as described by Suomalainen et al. (2013). Cells were imaged in PBS with a Leica SP5 confocal laser scanning microscope using a 63× magnification oil objective (numerical aperture 1.4) and zoom factor 2. A single slice through the middle of the cell was recorded for the DAPI channel, and stacks were recorded at 0.5-µm intervals for the 9C12 signal with 4× frame averaging. Numbers of cell-associated virus particles were determined from maximum projections of confocal stacks using a custom-programmed MatLab (The Mathworks) routine. Scatterplots were made using GraphPad Prism.

Detection efficiency of incoming EdC-labeled vDNA

To determine the number of EdC-labeled virus particles carrying a detectable vDNA signal, HeLa-ATCC MIB1-knockout cells were incubated with EdC-labeled AdV-C5 (m.o.i. ∼23,440 virus particles per cell) at 37°C for 60 min in DMEM supplemented with 0.2% BSA and penicillin-streptomycin, and, after removal of unbound virus, incubation

Journal of Cell Science (2021) 134, jcs252544. doi:10.1242/jcs.252544

was continued at 37°C for 60 min in DMEM supplemented with 7.5% FCS, 1% non-essential amino acids and penicillin-streptomycin before fixation. To tag virus particles, fixed cells were stained with 9C12 anti-hexon and secondary Alexa Fluor 594-conjugated anti-mouse (Thermo Fisher Scientific, A21203) antibodies, as described above and by Suomalainen et al. (2013). The viral vDNA was detected by a click reaction using Alexa Fluor 488-conjugated azide (Thermo Fisher Scientific, A10266) as previously described (Wang et al., 2013), and nuclei were stained with DAPI. The samples were imaged with a Leica SP5 confocal laser scanning microscope using a 63× magnification oil objective (numerical aperture 1.4) and zoom factor 2. Stacks were recorded for all channels at 0.5-µm intervals with sequential acquisition using between-frames switching mode and 3× frame averaging for the 9C12 signals and 4× frame averaging for vDNA signals. The sensitive Leica HyD hybrid detector was required for proper detection of the vDNA signals. A custom-programmed MatLab (The Mathworks) routine was used to determine the number of cell-associated virus particles from maximum projections of confocal stacks and to score vDNA signal on the virus particles. The threshold value for a positive vDNA signal was determined by overlaying a virus particle image and click reaction image obtained from cells infected with virus not labeled with EdC and taking the highest virus-associated signal in the click reaction image as a cutoff value.

To determine the efficiency of incoming vDNA detection in relation to increasing infection time, A549 cells were incubated with EdC-labeled AdV-C5 (m.o.i. ∼23,440) at 37°C for 60 min, as described above, and, after removal of unbound virus, incubation was continued at 37°C for an additional 2 or 6 h before fixation. The incoming viral vDNA was detected by a click reaction using azide–Alexa Fluor 488, Alexa Fluor 647 NHS Ester was used for staining of cell area and nuclei were stained with DAPI. The samples were imaged with a Leica SP5 confocal laser scanning microscope using a 63× magnification oil objective (numerical aperture 1.4) and zoom factor 2. Stacks were recorded at 1-µm intervals with sequential acquisition using between-stacks switching mode. Signals for vDNA were recorded with 6× frame averaging and with a Leica HyD hybrid detector in the normal mode. A CellProfiler pipeline was used to score vDNA puncta within the total cell area (Alexa Fluor 647 mask) and within the nuclear area (DAPI mask). To improve vDNA puncta segmentation, vDNA images were processed with the Fiji built-in plugin Rolling Ball Background Subtraction, with rolling ball radius set to 20 pixels, prior to running the CellProfiler pipeline. The resulting data were sorted using KNIME Analytics Platform, and GraphPad Prism was used for creating the scatter plots.

qPCR quantification of vDNA in infected cells

Confluent A549 cell cultures on a 6-well dish were incubated with AdV-C5 (m.o.i. ∼17,600) at 37°C for 60 min, as described above, and, after removal of unbound virus, incubation was continued at 37°C for an additional 2 or 6 h. Non-infected cells were used as a control. Cells were washed twice with PBS, scraped into 200 µl PBS, and total DNA was extracted using a DNeasy Blood and Tissue kit (Qiagen, 69506) according to a protocol recommended by the manufacturer. The DNA was eluted into 100 µl of the kit buffer AE. Quantification of the vDNA was performed using quantitative PCR with an ABI QuantStudio 3 real-time PCR system by setting up a three-step melt-curve analysis using primers E1A_forward (5′-GGTGGAGTTTGTGAC-GTGG-3′) and E1A_reverse (5′-CGCGCGAAAATTGTCACTTC-3′) against the Ad5 E1A promoter and enhancer DNA (Prasad et al., 2020). Viral genome copy numbers were estimated from a plasmid standard curve.

Relating E1A transcripts to vDNA at single-cell level

A549 cells were seeded at a density of 40,000 per well on Alcian Blue-coated coverslips in a 24-well plate format and grown for two days. EdC-labeled AdV-C5 was incubated with cells (m.o.i. ∼23,440 virus particles per cell) at 37°C for 60 min in DMEM supplemented with 0.2% BSA and penicillin-streptomycin. After removal of unbound virus, incubation was continued in DMEM supplemented with 7.5% FCS, 1% non-essential amino acids and penicillin-streptomycin for a further 7 h before fixation. RNA FISH with E1A probes was carried out as described above. Coverslips were subsequently inverted on 30 µl droplets of Image-iT FX Signal Enhancer (Thermo Fisher Scientific, I36933) and incubated at room temperature for 30 min. After two washes with PBS, a click reaction with Alexa Fluor 488-conjugated azide was performed as described by Wang et al. (2013). Nuclei were stained with DAPI and cell area with Alexa Fluor 647 NHS ester. Imaging was carried out with a Leica SP5 confocal laser scanning microscope using a 63× magnification oil objective (numerical aperture 1.4) and zoom factor 2.5. Stacks were recorded at 1-µm intervals with sequential acquisition using between-stacks switching mode and 3× or 6× frame averaging for E1A and vDNA signals, respectively. The sensitive Leica HyD hybrid detector in the normal mode was required for proper detection of the vDNA signals. Maximum projections of confocal stacks and a CellProfiler pipeline were used to determine the E1A transcript numbers in the cell area (Alexa Fluor 647 cell mask) and vDNA numbers in the total cell area (Alexa Fluor 647 cell mask) or the nuclear area (DAPI mask). Proper cell and nucleus segmentation was controlled and adjusted manually if necessary. The resulting data were sorted using KNIME Analytics Platform, and cells with no vDNA signal were excluded from the analysis. GraphPad Prism was used for producing the scatter plots and performing Spearman's correlation tests. For determining the effect of cell cycle for vDNA–E1A transcript number correlations, cells were first classified as G1 or S/G2/M cells according to their integrated nuclear DAPI intensities (see below) and the two cell populations were separately analyzed in GraphPad Prism for correlations between total cell-associated or nuclear vDNA counts and the number of E1A transcripts per cell. Representative images shown in figures are maximum projections of confocal stacks, and images were processed with Fiji, applying the same changes in brightness and contrast to all image groups in the series.

For the HDF-TERT experiment, cells were incubated with EdC-labeled AdV-C5 at 37°C for 15 h in DMEM supplemented with 10% FCS (m.o.i. ∼4800 virus particles per cell), 1% non-essential amino acids and penicillin-streptomycin. After removal of the inoculum medium, incubation was continued at 37°C for an additional 7 h before cells were fixed and processed as described above for the A549 infection.

Assigning cell cycle phase using integrated DAPI intensities

For determination of the cell cycle phase, cells were stained with DAPI, and imaging was performed with either wide-field high-throughput or confocal microscopy. The segmentation of the nucleus was performed using a CellProfiler pipeline and the DAPI intensities were measured over the nuclear mask. Following this, histograms of integrated DAPI intensities were plotted for infected and non-infected samples in statistical software JMP (JMP®, Version 13, SAS Institute Inc., Cary, NC, 1989-2007). The cells were called as G1 stage cells if their integrated DAPI intensities fell between the range determined by the visually selected cutoffs from the non-infected samples, as has been described before (Roukos et al., 2015). For example, in Fig. S3B, the threshold for G1-population cells was between 132–200 AU (arbitrary units). Cells outside this range were called S/G2/M phase cells.

Effect of the cell cycle on early accumulation of E1A transcripts

A549 cells grown on 96-well imaging plates were incubated with AdV-C5 at 37°C for 60 min (m.o.i. ∼54,400 virus particles per cell) in DMEM supplemented with 0.2% BSA and penicillin-streptomycin. After removal of unbound virus, incubation was continued at 37°C for an additional 3 or 6 h in DMEM supplemented with 7.5% FCS, 1% non-essential amino acids and penicillin-streptomycin. Fixed cells were stained with E1A probes, Alexa Fluor 647 NHS Ester was used for staining of the cell area and DAPI used for staining the nucleus as described above. Images were acquired with a Molecular Devices automated ImageXpress Micro XL wide-field imaging system using a 20× S Fluor objective (numerical aperture 0.75). Image stacks were acquired for RNA-FISH and cell area channels, and a single focal plane was acquired for DAPI. A CellProfiler pipeline was used for determining the nuclear DAPI intensities and the mean E1A transcript intensities at single-cell level from maximum projections of image stacks. The separation between G1 and S/G2/M phases was performed as described above, with a threshold of 132–200 AU. The histogram in Fig. 3B (distribution of E1A mRNA cytoplasmic intensities in G1 versus S versus G2 M) was drawn from a full dataset, whereas the scatterplot in Fig. 3B was

Journal of Cell Science (2021) 134, jcs252544. doi:10.1242/jcs.252544

drawn from a randomly sampled populations of 1659 and 1314 G1 and S/G2/M infected cells, respectively. Both the histogram and the scatter plot were made using JMP. The outliers of the E1A-expressing population were the cells that had intensities more than 1.5× the interquartile range from the 75th percentile.

Analysis of early E1A transcript accumulation in a G1-enriched cell population was performed in melanoma A375 cells, because these cells respond well to serum starvation. Cells were seeded on 96-well imaging plates at a density of 18,000 per well, and after one day incubation cells were switched to DMEM medium without FCS. After 19 h, AdV-C5 was added to cells at m.o.i. of ∼36,250 virus particles per cell for 60 min at 37°C in DMEM without FCS supplemented with penicillin-streptomycin. After removal of unbound virus, incubation was continued at 37°C for a further 9 h, either in DMEM without FCS supplemented with penicillin-streptomycin (starved+starved sample) or in DMEM supplemented with 7.5% FCS, 1% non-essential amino acids and penicillin-streptomycin (starved+serum sample). Cells were fixed and stained with E1A transcript probes and DAPI as described above. For determination of E1A transcript numbers per cell, a Molecular Devices automated ImageXpress Micro confocal imaging system and 40× Plan Apo Lambda objective (numerical aperture 0.95) was used for image acquisition with confocal stacks for the E1A channel, a single focal plane for DAPI and a transmission light image. For determination of the percentage of G1-phase cells in the different samples, a Molecular Devices automated ImageXpress Micro XL wide-field imaging system and 10× Plan Fluor objective (numerical aperture 0.3) was used for recording images in the DAPI channel. A CellProfiler pipeline was used for determining the nuclear DAPI intensities and the number of E1A transcripts per cell from maximum-projection image stacks (cell boundaries segmented from the transmission light images). The saved E1A and cell outline segmentation images from the CellProfiler pipeline were used to control proper segmentation, and cells erroneously having numerous mRNAs as a result of a spillover from a neighboring high-expressing cell were manually removed from the dataset. Cells with either ≥1 or ≥50 fluorescent E1A transcript puncta were included in the data analyses and boxplots from these cells were drawn using JMP. To check the efficiency of G1 accumulation by serum-starvation, histograms of equal numbers of randomly sampled cells (∼7500 cells) of indicated samples were plotted using their integrated DAPI intensity. Cells were scored as G1-phase cells if their integrated DNA intensity fell between the visually selected cutoff of 2–15 AU, and subsequently the percentage of G1-phase cells was calculated.

Comparison of the effect of the cell cycle on CMV immediate early and E1A promoter activities

HeLa-ATCC cells were seeded on 96-well imaging plates at a density of 10,000 cells/well and grown for one day. Plasmids containing an EGFP expression cassette under the control of AdV-C5 E1A or cytomegalovirus (CMV) promoter and enhancer regions (Prasad et al., 2020) were transfected at an amount of 100 ng/well using Lipofectamine 2000 transfection method (Thermo Fisher Scientific, 11668019). Cells were fixed 48 h post transfection, stained with DAPI and imaged with a Molecular Devices automated ImageXpress Micro XL widefield imaging system using a 20× S Fluor objective (numerical aperture 0.75) and a single focal plane for all channels. Nuclei of the cells were segmented using CellProfiler, and the EGFP signal was measured over this mask. Cells were scored as being in the G1 phase of the cell cycle if their integrated DNA intensity fell in the visually selected cutoff of 10–22 AU seen in non-transfected cells. Mean nuclear EGFP intensity in transfected cells was split into four equal frequency bins of increasing EGFP intensities, and cell cycle plots were drawn from these populations. An R script for the two-proportion *Z*-test was used to test whether the proportion of G1 cells in the highest EGFP expression bin was statistically different between the samples.

Effect of the cell cycle on E1A protein expression in HeLa-FUCCI cells

Hela-FUCCI cells were seeded on a 96-well imaging plate at a density of 7000 cells/well and grown for two days. AdV-C5 was incubated with cells at an m.o.i. of ∼11,200 virus particles per cell for 60 min at 37°C in DMEM supplemented with 0.2% BSA and penicillin-streptomycin. After removal of unbound virus, incubation was continued in DMEM supplemented with 7.5% FCS, 1% non-essential amino acids and penicillin-streptomycin for 9.5 h. Cells were fixed and stained with M58 anti-E1A (ThermoFisher Scientific, MA5-13643; 0.7 µg/ml) and secondary anti-mouse IgG Alexa Fluor 680-conjugated (Thermo Fisher Scientific, A21058) antibodies and DAPI as previously described (Suomalainen et al., 2013). Images were acquired with a Molecular Devices automated ImageXpress Micro XL wide-field imaging system using a 20× S Fluor objective (numerical aperture 0.75) and a single focal plane for all channels. Nuclear stain DAPI was used to segment nuclei using CellProfiler. The segmentation output was fed to CellProfiler Analyst (Jones et al., 2008), which was used to differentiate cells into early G1, G1, G1/S and S/G2/M phases of the cell cycle. HeLa-FUCCI cells express truncated forms of Kusabira orange-fused Cdt1 as a marker for early and late G1 phases, and Geminin fused to Azami Green as a marker for S and G2 phases of the cell cycle (Sakaue-Sawano et al., 2008). A short transition phase during the change from G1 (red) to S phase (green) is identified as G1/S phase and appears yellow due to the overlap of the two fluorescence signals. Using this set of rules, CellProfiler Analyst was trained to separate the cells into these phases and the output was re-examined to manually reassign erroneously identified phases. The software was re-trained until the output appeared satisfactory (Prasad et al., 2017). The scatter plots of mean E1A nuclear intensity expressed in different cell cycle stage cells were plotted in JMP.

Assaying transcriptionally active nuclear vDNAs

A549 cells were seeded at a density of 40,000 per well on Alcian Blue-coated coverslips in a 24-well plate format and grown for two days. EdC-labeled AdV-C5 was incubated with cells (m.o.i. ∼23,440 virus particles per cell) at 37°C for 60 min in DMEM supplemented with 0.2% BSA and penicillin-streptomycin. After removal of unbound virus, incubation was continued in DMEM supplemented with 7.5% FCS, 1% non-essential amino acids and penicillin-streptomycin for a further 13.5 or 15 h before fixation. Acetic acid (2.5%) was added to the PFA-fixative solution when nuclear transcription sites were analyzed. RNA-FISH staining with E4 intron probes (these probes also detect the E4orf1/orf2 mRNAs) and vDNA detection by click reaction were carried out as described above. RNase A treatment (50 µg/ml in PBS) was for 30 min at room temperature (control cells were kept in PBS), and cells were fixed again with 3% PFA in PBS for 15 min at room temperature before proceeding to the RNA FISH and click reactions. Nuclei were stained with DAPI, and cell area was stained for using Alexa Fluor 647 NHS ester. Imaging was carried out with a Leica SP5 confocal laser scanning microscope using a 63× magnification oil objective (numerical aperture 1.4) and zoom factor 2.5. Stacks were recorded at 1-µm intervals with sequential acquisition using between-frames switching mode and 3× or 4× line accumulation for vDNA signals. The sensitive Leica HyD hybrid detector in the normal mode was used for vDNA signals. Maximum projections of confocal stacks and the CellProfiler pipeline were used to determine the E4 transcript/intron signals in the cell cytoplasm (Alexa Fluor 647 cell mask minus DAPI nuclear area), as well as the number of nuclear E4 puncta or total and E4-positive vDNA numbers in the nuclear area (DAPI mask). To improve nuclear vDNA segmentation, vDNA images were processed with the Fiji plugin Rolling Ball Background Subtraction, with rolling ball radius set to 5 pixels, prior to running the CellProfiler pipeline. Proper cell and nucleus segmentation was controlled and adjusted manually if necessary. Proper vDNA and E4 puncta segmentations were checked from saved CellProfiler segmentation images. For setting threshold values for E4-positive vDNAs, background signal levels were first determined by placing vDNA images on E4 probe channel images of non-infected cells and the highest vDNA-associated E4 intensity was taken as the cutoff value. The selected cutoff value was compared to E4 intensity values obtained from visually selected E4-negative and -positive vDNAs to ascertain that the selected cutoff values correctly distinguished between E4-negative and -positive nuclear vDNAs. The data were sorted using KNIME Analytics Platform, and cells with no nuclear vDNA signal were excluded from the analysis. GraphPad Prism was used to produce the scatter plots. Representative images were produced using Fiji as described above.

Assaying progression of incoming vDNAs to a replication phase

A549 cells were infected with AdV-C5 at the indicated multiplicities of infection as described above. For labeling newly synthesized vDNAs, EdC (2.5 µM) was included in the culture medium for the last four hours before fixation, and viral replication centers were visualized with a click reaction using Alexa Fluor 488-conjugated azide. Cytosine arabinoside (AraC; Sigma-Aldrich, C3350000; final concentration 10 µg/ml), added after removal of unbound virus, was used for suppression of viral genome replication. When probing for nuclear targets of the E1A transcript probes, bDNA FISH was carried out as described above, except that 2.5% (v/v) glacial acetic acid was included in the fixative to improve probe detection of nuclear targets (Chartrand et al., 2000) and cells were treated with Affymetrix QuantiGene ViewRNA HC screening assay kit protease (1:4000 dilution, 10 min incubation at room temperature) after permeabilization with Triton X-100. The protease was inactivated by incubation in the kit protease stop buffer (10 min at room temperature). RNase A treatment for nuclear E1A probe signal was carried out after inactivation of protease as described above. S1 nuclease (Thermo Fisher Scientific, EN0321) treatment was carried out after inactivation of protease with 0.56 U/µl nuclease in S1 nuclease buffer (Thermo Fisher Scientific) for 60 min at 37°C followed by two washes with PBS, incubation with 3% paraformaldehyde in PBS for 20 min at room temperature and two washes with PBS before proceeding to the FISH staining. Control cells were incubated in S1 nuclease buffer without the nuclease. To identify incoming vDNAs that had proceeded to a replication phase, A549 cells were infected with EdC-labeled AdV-C5 (m.o.i. ∼23,400 virus particles per cell) as described above, and, after removal of unbound virus, incubation was continued at 37°C for an additional 27 h, with AraC in the culture medium during the last 20 h. The cells were fixed using 3% paraformaldehyde in PBS containing 2.5% acetic acid, permeabilized by Triton X-100 in PBS, treated with protease and stained with E1A probes, as described above, followed by incubation in Image-iT FX Signal Enhancer and click reaction with Alexa Fluor 488-conjugated azide as described above. Cells were also stained with DAPI and Alexa Fluor 647 NHS ester. Imaging was carried out with a Leica SP5 confocal laser scanning microscope as described above. Representative images shown are maximum projections of confocal stacks, processed in Fiji (Schindelin et al., 2012) by applying the same changes in brightness and contrast to all image groups in the series. Colocalization of nuclear E1A probe signal with vDNA signal was used for identification of incoming vDNAs that had proceeded to a replication phase. Alternatively, replication-phase vDNAs were identified by colocalization of anti-DBP signal with vDNA click reaction signal. Immunofluorescence staining with mouse anti-DBP (1:100; clone A1-6; kindly provided by Nancy Reich, Stony Brook University, Stony Brook, NY; Reich et al., 1983) and Alexa Fluor 594-conjugated anti-mouse IgG antibodies was carried out first, followed by a click reaction with Alexa Fluor 488-conjugated azide. Imaging was carried out with a Leica SP5 confocal laser scanning microscope as described above. Representative images shown are maximum projections of confocal stacks, processed in Fiji as described above.

Statistical analyses

Statistical analyses were performed either by Kolmogorov–Smirnov test using GraphPad Prism (Fig. 2A), by permutation tests using a custom-programmed R script (Fig. 3B,C; Fig. 4B and Fig. S1B), by Spearman's correlation coefficient using GraphPad Prism (Fig. 1E, Fig. 2C, Fig. 5; Fig. S2B,C) or by two-proportions *Z*-test using an R script (Fig. 4A). Alpha factor 0.001 and 5000 permutations were used in the permutation tests. This commonly resulted in a *P* value of 0. However, permutation *P* values should never be zero (Phipson and Smyth, 2010). Therefore, the *P* value was calculated using the recommended formula $P=(b+1)/(m+1)$, in which b is the number of permutations giving a difference greater than the observed difference between samples and m is the number of permutations.

Acknowledgements

We thank Patrick Hearing, Kathleen Rundell, Laurence Fayadat, Wiebe Olijve, Cornel Fraefel and Alex Hajnal for cell lines; Nancy Reich for antibodies; Nicole Meili and Melanie Grove for tissue culture; and the ZMB microscopy and image analysis core facility at the University of Zurich for advice with confocal microscopy.

Competing interests

The authors declare no competing or financial interests.

Author contributions

Conceptualization: M.S., V.P., U.F.G.; Methodology: M.S., V.P.; Software: V.P.; Validation: M.S., V.P., A.K.; Formal analysis: M.S., V.P., A.K., U.F.G.; Investigation: M.S., V.P., A.K.; Resources: M.S., V.P.; Data curation: M.S., V.P.; Writing - original draft: M.S.; Writing - review & editing: M.S., V.P., U.F.G.; Visualization: M.S., V.P.; Supervision: U.F.G.; Project administration: U.F.G.; Funding acquisition: U.F.G.

Funding

This work was supported by grants from the Schweizerischer Nationalfonds zur Förderung der Wissenschaftlichen Forschung (31003A_179256/1; 316030_170799/1; CRSII5_170929/1) and the Kanton Zurich.

Data availability

The data and scripts used to create the figures in this manuscript (maximum projections of raw images, CellProfiler pipelines and result Microsoft Excel files) are deposited at Mendeley Data (http://dx.doi.org/10.17632/r9t9dgg57k.2).

Supplementary information

Supplementary information available online at https://jcs.biologists.org/lookup/doi/10.1242/jcs.252544.supplemental

Peer review history

The peer review history is available online at https://jcs.biologists.org/lookup/doi/10.1242/jcs.252544.reviewer-comments.pdf

References

Bagga, S. and Bouchard, M. J. (2014). Cell cycle regulation during viral infection. *Methods Mol. Biol.* **1170**, 165-227. doi:10.1007/978-1-4939-0888-2_10

Battich, N., Stoeger, T. and Pelkmans, L. (2013). Image-based transcriptomics in thousands of single human cells at single-molecule resolution. *Nat. Methods* **10**, 1127-1133. doi:10.1038/nmeth.2657

Battich, N., Stoeger, T. and Pelkmans, L. (2015). Control of Transcript Variability in Single Mammalian Cells. *Cell* **163**, 1596-1610. doi:10.1016/j.cell.2015.11.018

Bauer, M., Flatt, J. W., Seiler, D., Cardel, B., Emmenlauer, M., Boucke, K., Suomalainen, M., Hemmi, S. and Greber, U. F. (2019). The E3 Ubiquitin Ligase Mind Bomb 1 Controls Adenovirus Genome Release at the Nuclear Pore Complex. *Cell Rep.*, **29**, 3785-3795e8. doi:10.1016/j.celrep.2019.11.064

Ben-Israel, H. and Kleinberger, T. (2002). Adenovirus and cell cycle control. *Front. Biosci.* **7**, d1369-d1395. doi:10.2741/ben

Bercovich-Kinori, A., Tai, J., Gelbart, I. A., Shitrit, A., Ben-Moshe, S., Drori, Y., Itzkovitz, S., Mandelboim, M. and Stern-Ginossar, N. (2016). A systematic view on influenza induced host shutoff. *eLife*, **5**, e18311. doi: 10.7554/eLife.18311

Berk, A. J. (1986). Adenovirus promoters and E1A transactivation. *Annu. Rev. Genet.* **20**, 45-79. doi:10.1146/annurev.ge.20.120186.000401

Berk, A. J. (2005). Recent lessons in gene expression, cell cycle control, and cell biology from adenovirus. *Oncogene* **24**, 7673-7685. doi:10.1038/sj.onc.1209040

Binger, M. H. and Flint, S. J. (1984). Accumulation of early and intermediate mRNA species during subgroup C adenovirus productive infections. *Virology* **136**, 387-403. doi:10.1016/0042-6822(84)90175-2

Bolwig, G. M., Bruder, J. T. and Hearing, P. (1992). Different binding site requirements for binding and activation for the bipartite enhancer factor EF-1A. *Nucleic Acids Res.* **20**, 6555-6564. doi:10.1093/nar/20.24.6555

Brightwell, G., Poirier, V., Cole, E., Ivins, S. and Brown, K. W. (1997). Serum-dependent and cell cycle-dependent expression from a cytomegalovirus-based mammalian expression vector. *Gene* **194**, 115-123. doi:10.1016/S0378-1119(97)00178-9

Buettner, F., Natarajan, K. N., Casale, F. P., Proserpio, V., Scialdone, A., Theis, F. J., Teichmann, S. A., Marioni, J. C. and Stegle, O. (2015). Computational analysis of cell-to-cell heterogeneity in single-cell RNA-sequencing data reveals hidden subpopulations of cells. *Nat. Biotechnol.* **33**, 155-160. doi:10.1038/nbt.3102

Burckhardt, C. J., Suomalainen, M., Schoenenberger, P., Boucke, K., Hemmi, S. and Greber, U. F. (2011). Drifting motions of the adenovirus receptor Car and immobile integrins initiate virus uncoating and membrane lytic protein exposure. *Cell Host Microbe* **10**, 105-117. doi:10.1016/j.chom.2011.07.006

Carpenter, A. E., Jones, T. R., Lamprecht, M. R., Clarke, C., Kang, I. H., Friman, O., Guertin, D. A., Chang, J. H., Lindquist, R. A., Moffat, J. et al. (2006). CellProfiler: image analysis software for identifying and quantifying cell phenotypes. *Genome Biol.* **7**, R100. doi:10.1186/gb-2006-7-10-r100

Chartrand, P., Bertrand, E., Singer, R. H. and Long, R. M. (2000). Sensitive and high-resolution detection of RNA in situ. *Methods Enzymol.* **318**, 493-506. doi:10.1016/S0076-6879(00)18072-3

Chen, J., Morral, N. and Engel, D. A. (2007). Transcription releases protein VII from adenovirus chromatin. *Virology* **369**, 411-422. doi:10.1016/j.virol.2007.08.012

Chen, K. H., Boettiger, A. N., Moffitt, J. R., Wang, S. and Zhuang, X. (2015). RNA imaging. Spatially resolved, highly multiplexed RNA profiling in single cells. *Science* **348**, aaa6090.
Cho, W. K., Jayanth, N., English, B. P., Inoue, T., Andrews, J. O., Conway, W., Grimm, J. B., Spille, J. H., Lavis, L. D., Lionnet, T. et al. (2016). RNA Polymerase II cluster dynamics predict mRNA output in living cells. *eLife* **5**, e13617. doi:10.7554/eLife.13617
Cho, W.-K., Spille, J.-H., Hecht, M., Lee, C., Li, C., Grube, V. and Cisse, I. I. (2018). Mediator and RNA polymerase II clusters associate in transcription-dependent condensates. *Science* **361**, 412-415. doi:10.1126/science.aar4199
Chong, S., Dugast-Darzacq, C., Liu, Z., Dong, P., Dailey, G. M., Cattoglio, C., Heckert, A., Banala, S., Lavis, L., Darzacq, X. et al. (2018). Imaging dynamic and selective low-complexity domain interactions that control gene transcription. *Science* **361**, eaar2555. doi:10.1126/science.aar2555
Cisse, I. I., Izeddin, I., Causse, S. Z., Boudarene, L., Senecal, A., Muresan, L., Dugast-Darzacq, C., Hajj, B., Dahan, M. and Darzacq, X. (2013). Real-time dynamics of RNA polymerase II clustering in live human cells. *Science* **341**, 664-667. doi:10.1126/science.1239053
Crisostomo, L., Soriano, A. M., Mendez, M., Graves, D. and Pelka, P. (2019). Temporal dynamics of adenovirus 5 gene expression in normal human cells. *PLoS One* **14**, e0211192. doi:10.1371/journal.pone.0211192
Drayman, N., Patel, P., Vistain, L. and Tay, S. (2019). HSV-1 single cell analysis reveals anti-viral and developmental programs activation in distinct sub-populations. *eLife* **8**, e46339. doi:10.7554/eLife.46339
Ferro, A., Mestre, T., Carneiro, P., Sahumbaiev, I., Seruca, R. and Sanches, J. M. (2017). Blue intensity matters for cell cycle profiling in fluorescence DAPI-stained images. *Lab. Investig.* **97**, 615-625. doi:10.1038/labinvest.2017.13
Flint, S. J. and Sharp, P. A. (1976). Adenovirus transcription. V. Quantitation of viral RNA sequences in adenovirus 2-infected and transformed cells. *J. Mol. Biol.* **106**, 749-774.
Giberson, A. N., Davidson, A. R. and Parks, R. J. (2012). Chromatin structure of adenovirus DNA throughout infection. *Nucleic Acids Res.* **40**, 2369-2376. doi:10.1093/nar/gkr1076
Glenn, G. M. and Ricciardi, R. P. (1988). Detailed kinetics of adenovirus type-5 steady-state transcripts during early infection. *Virus Res.* **9**, 73-91. doi:10.1016/0168-1702(88)90051-2
Golumbeanu, M., Cristinelli, S., Rato, S., Munoz, M., Cavassini, M., Beerenwinkel, N. and Ciuffi, A. (2018). Single-Cell RNA-Seq Reveals Transcriptional Heterogeneity in Latent and Reactivated Hiv-Infected Cells. *Cell Rep.* **23**, 942-950. doi:10.1016/j.celrep.2018.03.102
Greber, U. F., Willetts, M., Webster, P. and Helenius, A. (1993). Stepwise dismantling of adenovirus 2 during entry into cells. *Cell* **75**, 477-486. doi:10.1016/0092-8674(93)90382-Z
Haruki, H., Gyurcsik, B., Okuwaki, M. and Nagata, K. (2003). Ternary complex formation between DNA-adenovirus core protein VII and TAF-Ibeta/SET, an acidic molecular chaperone. *FEBS Lett.* **555**, 521-527. doi:10.1016/S0014-5793(03)01336-X
Hearing, P. and Shenk, T. (1985). Sequence-independent autoregulation of the adenovirus type 5 E1A transcription unit. *Mol. Cell. Biol.* **5**, 3214-3221. doi:10.1128/MCB.5.11.3214
Heist, T., Fukaya, T. and Levine, M. (2019). Large distances separate coregulated genes in living Drosophila embryos. *Proc. Natl Acad. Sci. USA* **116**, 15062-15067. doi:10.1073/pnas.1908962116
Heldt, F. S., Kupke, S. Y., Dorl, S., Reichl, U. and Frensing, T. (2015). Single-cell analysis and stochastic modelling unveil large cell-to-cell variability in influenza A virus infection. *Nat. Commun.* **6**, 8938. doi:10.1038/ncomms9938
Hendrickx, R., Stichling, N., Koelen, J., Kuryk, L., Lipiec, A. and Greber, U. F. (2014). Innate Immunity to Adenovirus. *Hum. Gene. Ther.* **25**, 265-284. doi:10.1089/hum.2014.001
Hoeben, R. C. and Uil, T. G. (2013). Adenovirus DNA replication. *Cold Spring Harb. Perspect. Biol.* **5**, a013003. doi:10.1101/cshperspect.a013003
Hu, M.-C. and Hsu, M.-T. (1997). Adenovirus E1B 19K protein is required for efficient DNA replication in U937 cells. *Virology* **227**, 295-304. doi:10.1006/viro.1996.8349
Iftode, C. and Flint, S. J. (2004). Viral DNA synthesis-dependent titration of a cellular repressor activates transcription of the human adenovirus type 2 IVa2 gene. *Proc. Natl Acad. Sci. USA* **101**, 17831-17836. doi:10.1073/pnas.0407786101
Jones, T., Kang, I., Wheeler, D., Lindquist, R., Papallo, A., Sabatini, D., Golland, P. and Carpenter, A. (2008). CellProfiler Analyst: data exploration and analysis software for complex image-based screens. *BMC Bioinformatics* **9**, 1.
Karen, K. A. and Hearing, P. (2011). Adenovirus core protein VII protects the viral genome from a DNA damage response at early times after infection. *J. Virol.* **85**, 4135-4142. doi:10.1128/JVI.02540-10
Kato, S. E., Chahal, J. S. and Flint, S. J. (2012). Reduced infectivity of adenovirus type 5 particles and degradation of entering viral genomes associated with incomplete processing of the preterminal protein. *J. Virol.* **86**, 13554-13565. doi:10.1128/JVI.02337-12
King, B. R., Samacoits, A., Eisenhauer, P. L., Ziegler, C. M., Bruce, E. A., Zenklusen, D., Zimmer, C., Mueller, F. and Botten, J. (2018a). Visualization of Arenavirus RNA Species in Individual Cells by Single-Molecule Fluorescence In Situ Hybridization Suggests a Model of Cyclical Infection and Clearance during Persistence. *J. Virol.* **92**, e02241-17. doi:10.1128/JVI.02241-17
King, C. R., Zhang, A., Tessier, T. M., Gameiro, S. F. and Mymryk, J. S. (2018b). Hacking the Cell: Network Intrusion and Exploitation by Adenovirus E1A. *MBio.* **9**, e00390-18. doi:10.1128/mBio.00390-18
Komatsu, T., Haruki, H. and Nagata, K. (2011). Cellular and viral chromatin proteins are positive factors in the regulation of adenovirus gene expression. *Nucleic Acids Res.* **39**, 889-901. doi:10.1093/nar/gkq783
Krzywkowski, T., Ciftci, S., Assadian, F., Nilsson, M. and Punga, T. (2017). Simultaneous Single-Cell *In Situ* Analysis of Human Adenovirus Type 5 DNA and mRNA Expression Patterns in Lytic and Persistent Infection. *J. Virol.* **91**, e00166-17. doi:10.1128/JVI.00166-17
Larsson, A. J. M., Johnsson, P., Hagemann-Jensen, M., Hartmanis, L., Faridani, O. R., Reinius, B., Segerstolpe, A., Rivera, C. M., Ren, B. and Sandberg, R. (2019). Genomic encoding of transcriptional burst kinetics. *Nature* **565**, 251-254. doi:10.1038/s41586-018-0836-1
Lavery, D. J. and Chen-Kiang, S. (1990). Adenovirus E1A and E1B genes are regulated posttranscriptionally in human lymphoid cells. *J. Virol.* **64**, 5349-5359. doi:10.1128/JVI.64.11.5349-5359.1990
Levesque, M. J. and Raj, A. (2013). Single-chromosome transcriptional profiling reveals chromosomal gene expression regulation. *Nat. Methods* **10**, 246-248. doi:10.1038/nmeth.2372
Li, J., Dong, A., Saydaminova, K., Chang, H., Wang, G., Ochiai, H., Yamamoto, T. and Pertsinidis, A. (2019). Single-Molecule Nanoscopy Elucidates RNA Polymerase II Transcription at Single Genes in Live Cells. *Cell* **178**, 491-506e28.
Lieberman, P. M. (2016). Epigenetics and Genetics of Viral Latency. *Cell Host Microbe* **19**, 619-628. doi:10.1016/j.chom.2016.04.008
Lion, T. (2014). Adenovirus infections in immunocompetent and immunocompromised patients. *Clin. Microbiol. Rev.* **27**, 441-462. doi:10.1128/CMR.00116-13
Lubeck, E., Coskun, A. F., Zhiyentayev, T., Ahmad, M. and Cai, L. (2014). Single-cell in situ RNA profiling by sequential hybridization. *Nat. Methods* **11**, 360-361. doi:10.1038/nmeth.2892
Luisoni, S., Suomalainen, M., Boucke, K., Tanner, L. B., Wenk, M. R., Guan, X. L., Grzybek, M., Coskun, U. and Greber, U. F. (2015). Co-option of Membrane Wounding Enables Virus Penetration into Cells. *Cell Host Microbe* **18**, 75-85. doi:10.1016/j.chom.2015.06.006
Miller, D. L., Myers, C. L., Rickards, B., Coller, H. A. and Flint, S. J. (2007). Adenovirus type 5 exerts genome-wide control over cellular programs governing proliferation, quiescence, and survival. *Genome Biol.* **8**, R58. doi:10.1186/gb-2007-8-4-r58
Miller, M. S., Pelka, P., Fonseca, G. J., Cohen, M. J., Kelly, J. N., Barr, S. D., Grand, R. J., Turnell, A. S., Whyte, P. and Mymryk, J. S. (2012). Characterization of the 55-residue protein encoded by the 9S E1A mRNA of species C adenovirus. *J. Virol.* **86**, 4222-4233. doi:10.1128/JVI.06399-11
Montell, C., Fisher, E. F., Caruthers, M. H. and Berk, A. J. (1982). Resolving the functions of overlapping viral genes by site-specific mutagenesis at a mRNA splice site. *Nature* **295**, 380-384. doi:10.1038/295380a0
Moreau, P., Cournac, A., Palumbo, G. A., Marbouty, M., Mortaza, S., Thierry, A., Cairo, S., Lavigne, M., Koszul, R. and Neuveut, C. (2018). Tridimensional infiltration of DNA viruses into the host genome shows preferential contact with active chromatin. *Nat. Commun.* **9**, 4268. doi:10.1038/s41467-018-06739-4
Morris, S. J., Scott, G. E. and Leppard, K. N. (2010). Adenovirus late-phase infection is controlled by a novel L4 promoter. *J. Virol.* **84**, 7096-7104. doi:10.1128/JVI.00107-10
Oko, L. M., Kimball, A. K., Kaspar, R. E., Knox, A. N., Coleman, C. B., Rochford, R., Chang, T., Alderete, B., Van Dyk, L. F. and Clambey, E. T. (2019). Multidimensional analysis of Gammaherpesvirus RNA expression reveals unexpected heterogeneity of gene expression. *PLoS Pathog.* **15**, e1007849. doi:10.1371/journal.ppat.1007849
Oldstone, M. B. (2006). Viral persistence: parameters, mechanisms and future predictions. *Virology* **344**, 111-118. doi:10.1016/j.virol.2005.09.028
Ostapchuk, P., Suomalainen, M., Zheng, Y., Boucke, K., Greber, U. F. and Hearing, P. (2017). The adenovirus major core protein VII is dispensable for virion assembly but is essential for lytic infection. *PLoS Pathog.* **13**, e1006455. doi:10.1371/journal.ppat.1006455
Pelka, P., Ablack, J. N., Fonseca, G. J., Yousef, A. F. and Mymryk, J. S. (2008). Intrinsic structural disorder in adenovirus E1A: a viral molecular hub linking multiple diverse processes. *J. Virol.* **82**, 7252-7263. doi:10.1128/JVI.00104-08
Peng, K., Muranyi, W., Glass, B., Laketa, V., Yant, S. R., Tsai, L., Cihlar, T., Muller, B. and Krausslich, H. G. (2014). Quantitative microscopy of functional HIV post-entry complexes reveals association of replication with the viral capsid. *eLife* **3**, e04114. doi:10.7554/eLife.04114
Phipson, B. and Smyth, G. K. (2010). Permutation P-values should never be zero: calculating exact P-values when permutations are randomly drawn. *Stat. Appl. Genet. Mol. Biol.* **9**, 39. doi:10.2202/1544-6115.1585
Pied, N. and Wodrich, H. (2019). Imaging the adenovirus infection cycle. *FEBS Lett.* **593**, 3419-3448. doi:10.1002/1873-3468.13690

Prasad, V., Suomalainen, M., Hemmi, S. and Greber, U. F. (2017). Cell Cycle-Dependent Kinase Cdk9 Is a Postexposure Drug Target against Human Adenoviruses. *ACS Infect Dis.* **3**, 398-405. doi:10.1021/acsinfecdis.7b00009

Prasad, V., Suomalainen, M., Jasiqi, Y., Hemmi, S., Hearing, P., Hosie, L., Burgert, H.-G. and Greber, U. F. (2020). The UPR sensor IRE1alpha and the adenovirus E3-19K glycoprotein sustain persistent and lytic infections. *Nat. Commun.* **11**, 1997. doi:10.1038/s41467-020-15844-2

Prasad, V., Suomalainen, M., Pennauer, M., Yakimovich, A., Andriasyan, V., Hemmi, S. and Greber, U. F. (2014). Chemical Induction of Unfolded Protein Response Enhances Cancer Cell Killing through Lytic Virus Infection. *J. Virol.* **88**, 13086-13098. doi:10.1128/JVI.02156-14

Puray-Chavez, M., Tedbury, P. R., Huber, A. D., Ukah, O. B., Yapo, V., Liu, D., Ji, J., Wolf, J. J., Engelman, A. N. and Sarafianos, S. G. (2017). Multiplex single-cell visualization of nucleic acids and protein during HIV infection. *Nat. Commun.* **8**, 1882. doi:10.1038/s41467-017-01693-z

Raj, A., Peskin, C. S., Tranchina, D., Vargas, D. Y. and Tyagi, S. (2006). Stochastic mRNA synthesis in mammalian cells. *PLoS Biol.* **4**, e309. doi:10.1371/journal.pbio.0040309

Reich, N. C., Sarnow, P., Duprey, E. and Levine, A. J. (1983). Monoclonal antibodies which recognize native and denatured forms of the adenovirus DNA-binding protein. *Virology* **128**, 480-484. doi:10.1016/0042-6822(83)90274-X

Rodriguez, J., Ren, G., Day, C. R., Zhao, K., Chow, C. C. and Larson, D. R. (2019). Intrinsic Dynamics of a Human Gene Reveal the Basis of Expression Heterogeneity. *Cell* **176**, 213-226e18.

Roukos, V., Pegoraro, G., Voss, T. C. and Misteli, T. (2015). Cell cycle staging of individual cells by fluorescence microscopy. *Nat. Protoc.* **10**, 334-348. doi:10.1038/nprot.2015.016

Russell, A. B., Trapnell, C. and Bloom, J. D. (2018). Extreme heterogeneity of influenza virus infection in single cells. *eLife* **7**, e32303. doi:10.7554/eLife.32303

Russell, A. B., Elshina, E., Kowalsky, J. R., Te Velthuis, A. J. W. and Bloom, J. D. (2019). Single-Cell Virus Sequencing of Influenza Infections That Trigger Innate Immunity. *J. Virol.* **93**, e00500-19. doi:10.1128/JVI.00500-19

Sabari, B. R., Dall'Agnese, A., Boija, A., Klein, I. A., Coffey, E. L., Shrinivas, K., Abraham, B. J., Hannett, N. M., Zamudio, A. V., Manteiga, J. C. et al. (2018). Coactivator condensation at super-enhancers links phase separation and gene control. *Science* **361**, eaar3958. doi:10.1126/science.aar3958

Sakaue-Sawano, A., Kurokawa, H., Morimura, T., Hanyu, A., Hama, H., Osawa, H., Kashiwagi, S., Fukami, K., Miyata, T., Miyoshi, H. et al. (2008). Visualizing spatiotemporal dynamics of multicellular cell-cycle progression. *Cell* **132**, 487-498. doi:10.1016/j.cell.2007.12.033

Schindelin, J., Arganda-Carreras, I., Frise, E., Kaynig, V., Longair, M., Pietzsch, T., Preibisch, S., Rueden, C., Saalfeld, S., Schmid, B. et al. (2012). Fiji: an open-source platform for biological-image analysis. *Nat. Methods* **9**, 676-682. doi:10.1038/nmeth.2019

Schümann, M. and Dobbelstein, M. (2006). Adenovirus-induced extracellular signal-regulated kinase phosphorylation during the late phase of infection enhances viral protein levels and virus progeny. *Cancer Res.* **66**, 1282-1288. doi:10.1158/0008-5472.CAN-05-1484

Shah, S., Takei, Y., Zhou, W., Lubeck, E., Yun, J., Eng, C. L., Koulena, N., Cronin, C., Karp, C., Liaw, E. J. et al. (2018). Dynamics and Spatial Genomics of the Nascent Transcriptome by Intron seqFISH. *Cell* **174**, 363-376e16.

Shaw, A. R. and Ziff, E. B. (1980). Transcripts from the adenovirus-2 major late promoter yield a single early family of 3′ coterminal mRNAs and five late families. *Cell* **22**, 905-916. doi:10.1016/0092-8674(80)90568-1

Spector, D. J., Mcgrogan, M. and Raskas, H. J. (1978). Regulation of the appearance of cytoplasmic RNAs from region 1 of the adenovirus 2 genome. *J. Mol. Biol.* **126**, 395-414. doi:10.1016/0022-2836(78)90048-7

Steuerman, Y., Cohen, M., Peshes-Yaloz, N., Valadarsky, L., Cohn, O., David, E., Frishberg, A., Mayo, L., Bacharach, E., Amit, I. et al. (2018). Dissection of Influenza Infection In Vivo by Single-Cell RNA Sequencing. *Cell Syst.* **6**, 679-691e4.

Stichling, N., Suomalainen, M., Flatt, J. W., Schmid, M., Pacesa, M., Hemmi, S., Jungraithmayr, W., Maler, M. D., Freudenberg, M. A., Plückthun, A. et al. (2018). Lung macrophage scavenger receptor SR-A6 (MARCO) is an adenovirus type-specific virus entry receptor. *PLoS Pathog.* **14**, e1006914. doi:10.1371/journal.ppat.1006914

Strunze, S., Engelke, M. F., Wang, I.-H., Puntener, D., Boucke, K., Schleich, S., Way, M., Schoenenberger, P., Burckhardt, C. J. and Greber, U. F. (2011). Kinesin-1-mediated capsid disassembly and disruption of the nuclear pore complex promote virus infection. *Cell Host Microbe* **10**, 210-223. doi:10.1016/j.chom.2011.08.010

Suomalainen, M., Luisoni, S., Boucke, K., Bianchi, S., Engel, D. A. and Greber, U. F. (2013). A direct and versatile assay measuring membrane penetration of adenovirus in single cells. *J. Virol.* **87**, 12367-12379. doi:10.1128/JVI.01833-13

Sweeney, J. A. and Hennessey, J. P.Jr. (2002). Evaluation of accuracy and precision of adenovirus absorptivity at 260 nm under conditions of complete DNA disruption. *Virology* **295**, 284-288. doi:10.1006/viro.2002.1406

Tang, L. S. Y., Covert, E., Wilson, E. and Kottilil, S. (2018). Chronic Hepatitis B Infection: A Review. *JAMA* **319**, 1802-1813. doi:10.1001/jama.2018.3795

Triemer, T., Messikommer, A., Glasauer, S. M. K., Alzeer, J., Paulisch, M. H. and Luedtke, N. W. (2018). Superresolution imaging of individual replication forks reveals unexpected prodrug resistance mechanism. *Proc. Natl. Acad. Sci. USA* **115**, E1366-E1373. doi:10.1073/pnas.1714790115

Tyagi, S. (2009). Imaging intracellular RNA distribution and dynamics in living cells. *Nat. Methods* **6**, 331-338. doi:10.1038/nmeth.1321

Vahey, M. D. and Fletcher, D. A. (2019). Low-Fidelity Assembly of Influenza A Virus Promotes Escape from Host Cells. *Cell* **176**, 281-294e19.

Varghese, R., Mikyas, Y., Stewart, P. L. and Ralston, R. (2004). Postentry neutralization of adenovirus type 5 by an antihexon antibody. *J. Virol.* **78**, 12320-12332. doi:10.1128/JVI.78.22.12320-12332.2004

Voelkerding, K. and Klessig, D. F. (1986). Identification of two nuclear subclasses of the adenovirus type 5-encoded DNA-binding protein. *J. Virol.* **60**, 353-362. doi:10.1128/JVI.60.2.353-362.1986

Wang, I. H., Suomalainen, M., Andriasyan, V., Kilcher, S., Mercer, J., Neef, A., Luedtke, N. W. and Greber, U. F. (2013). Tracking viral genomes in host cells at single-molecule resolution. *Cell Host Microbe* **14**, 468-480. doi:10.1016/j.chom.2013.09.004

Wang, I.-H., Burckhardt, C. J., Yakimovich, A., Morf, M. K. and Greber, U. F. (2017). The nuclear export factor CRM1 controls juxta-nuclear microtubule-dependent virus transport. *J. Cell Sci.* **130**, 2185-2195. doi:10.1242/jcs.203794

Wichgers Schreur, P. J. and Kortekaas, J. (2016). Single-Molecule FISH Reveals Non-selective Packaging of Rift Valley Fever Virus Genome Segments. *PLoS Pathog.* **12**, e1005800. doi:10.1371/journal.ppat.1005800

Wilson, M. C. and Darnell, J. E.Jr. (1981). Control of messenger RNA concentration by differential cytoplasmic half-life. Adenovirus messenger RNAs from transcription units 1A and 1B. *J. Mol. Biol.* **148**, 231-251. doi:10.1016/0022-2836(81)90537-4

Xin, X., Wang, H., Han, L., Wang, M., Fang, H., Hao, Y., Li, J., Zhang, H., Zheng, C. and Shen, C. (2018). Single-Cell Analysis of the Impact of Host Cell Heterogeneity on Infection with Foot-and-Mouth Disease Virus. *J. Virol.* **92**, e00179-18. doi:10.1128/JVI.00179-18

Xue, Y., Johnson, J. S., Ornelles, D. A., Lieberman, J. and Engel, D. A. (2005). Adenovirus protein VII functions throughout early phase and interacts with cellular proteins SET and pp32. *J. Virol.* **79**, 2474-2483. doi:10.1128/JVI.79.4.2474-2483.2005

Yakimovich, A., Andriasyan, V., Witte, R., Wang, I.-H., Prasad, V., Suomalainen, M. and Greber, U. F. (2015). Plaque2.0 – A High-Throughput Analysis Framework to Score Virus-Cell Transmission and Clonal Cell Expansion. *PLoS One* **10**, e0138760. doi:10.1371/journal.pone.0138760

Yu, J., Boyapati, A. and Rundell, K. (2001). Critical role for SV40 small-t antigen in human cell transformation. *Virology* **290**, 192-198. doi:10.1006/viro.2001.1204

Zanini, F., Pu, S. Y., Bekerman, E., Einav, S. and Quake, S. R. (2018). Single-cell transcriptional dynamics of flavivirus infection. *eLife* **7**, e32942. doi:10.7554/eLife.32942

Zhao, H., Dahlö, M., Isaksson, A., Syvänen, A.-C. and Pettersson, U. (2012). The transcriptome of the adenovirus infected cell. *Virology* **424**, 115-128. doi:10.1016/j.virol.2011.12.006

Zhao, H., Chen, M. and Pettersson, U. (2014). A new look at adenovirus splicing. *Virology* **456-457**, 329-341. doi:10.1016/j.virol.2014.04.006

Zheng, Y., Stamminger, T. and Hearing, P. (2016). E2F/Rb Family Proteins Mediate Interferon Induced Repression of Adenovirus Immediate Early Transcription to Promote Persistent Viral Infection. *PLoS Pathog.* **12**, e1005415. doi:10.1371/journal.ppat.1005415